LAWRENCE
LIVERMORE
NATIONAL
LABORATORY

LLNL-JRNL-484642

Detailed chemical kinetic reaction mechanisms for soy and rapeseed biodiesel fuels

C. K. Westbrook, C. V. Naik, O. Herbinet, W. J. Pitz, M. Mehl, S. M. Sarathy, H. J. Curran

May 23, 2011

Combustion and Flame

Disclaimer

Detailed Chemical Kinetic Reaction Mechanisms for Soy and Rapeseed Biodiesel Fuels

C. K. Westbrook†, C. V. Naik*, O. Herbinet#
W. J. Pitz†, M. Mehl†, M. Sarathy†, H. J. Curran&

Abstract

A detailed chemical kinetic reaction mechanism is developed for the five major components of soy biodiesel and rapeseed biodiesel fuels. These components, methyl stearate, methyl oleate, methyl linoleate, methyl linolenate, and methyl palmitate, are large methyl ester molecules, some with carbon-carbon double bonds, and kinetic mechanisms for them as a family of fuels have not previously been available. Of particular importance in these mechanisms are models for alkylperoxy radical isomerization reactions in which a C=C double bond is embedded in the transition state ring. The resulting kinetic model is validated through comparisons between predicted results and a relatively small experimental literature. The model is also used in simulations of biodiesel oxidation in jet-stirred reactor and intermediate shock tube ignition and oxidation conditions to demonstrate the capabilities and limitations of these mechanisms. Differences in combustion properties between the two biodiesel fuels, derived from soy and rapeseed oils, are traced to the differences in the relative amounts of the same five methyl ester components.

† Lawrence Livermore National Laboratory, Livermore, CA 94551
* Reaction Design, 6440 Lusk Blvd., Suite D205, San Diego, CA 92121
# Nancy Universite, CNRS, ENSIC, 1 rue Grandville, Nancy, France
& Chemistry Department, National University of Ireland, Galway, Ireland

Keywords: Biofuels; Reaction mechanisms; Chemical kinetics

INTRODUCTION

Fuels derived from plant oils [1, 2] have emerged in recent years as viable supplements or replacements for petroleum-based fuels. There is still considerable uncertainty about many aspects of bio-derived fuels, ranging from the capacity to produce large amounts of such fuels, the economics of producing them, and the impacts of removing plant products from animal and human food chains. At the same time, it is important to assess the combustion aspects of bio-derived fuels to compare them to more conventional fuels, including their ignition, oxidation, and potential for toxic emissions, and there are many such experimental studies taking place. Computer simulations of such combustion processes, including chemical kinetic studies, can be used to carry out some of these studies, accompanied by laboratory and engine experiments.

Chemical kinetic modeling studies require a detailed kinetic reaction mechanism for the components of a fuel and the intermediate chemical species that are produced during combustion, as the fuel is converted to final products. Bio-derived fuels are similar to petroleum-based fuels in that their final products are primarily carbon dioxide and water, but there are many intermediate species produced during biofuel combustion that are not present in combustion of more conventional fuels. In addition, in contrast with petroleum-based fuels, biofuels contain oxygen atoms within the primary fuel molecules, which can change the rates and reaction pathways of ignition and oxidation processes and can produce additional, different chemical pollutant emissions. For example, oxygen atoms in the biofuels have been shown to reduce soot production in diesel engines, both in engine experiments [3] and in kinetic modeling analysis [4], and biofuels may also affect engine emissions of nitrogen oxides [1,5]. A recent very thorough review of the effect of biodiesel fuels on diesel engine emissions has been

published by Lapuerta et al. [6], which not only summarizes current observations of these effects but also offers possible explanations for these observations. These observations are presented primarily in terms of how the incorporation of biodiesel fuel to conventional diesel fuel results in changes in engine operating conditions. Lapuerta et al. describe how adding biodiesel fuel to conventional diesel fuel leads to changes in injection timing, fuel viscosity, energy density due to the presence of O atoms in biodiesel fuels, reduced aromatic content, lower sulfur content of biodiesel fuels, and others as well, all correlated with the amount of biodiesel fuel added. In contrast, the present work shows how changes in chemical kinetic properties due to variations in biodiesel fuel composition affect some features of diesel engine combustion. These and other distinctions must be properly described by a detailed chemical kinetic reaction mechanism. Furthermore, since biofuels are most commonly used as additives to conventional hydrocarbon fuels, a combined reaction mechanism for a mixture of biofuels and petroleum fuels would require all of the kinetic features of both types of fuels, making such mechanisms extremely large and complex.

Some bio-derived fuels can be used to supplement conventional gasoline for use in spark-ignition engines, fuels including ethanol and butanol, while other types of bio-derived fuels are most useful as supplements or replacements for conventional fuels in diesel engine combustion. The present study is directed towards understanding the combustion of biofuels intended for use in diesel engine environments, specifically those large methyl ester species commonly used as biodiesel fuels.

Biodiesel fuels can be produced from a wide variety of vegetable oils [1,2]. Each plant oil has a somewhat unique variety of large acid molecules in its oil, and these distinctions are

retained when the oils are converted to large alkyl esters via the well-known esterification process [2]. When methanol is used in the esterification process, these components are large methyl esters, each with a long linear chain of carbon atoms. Some of these carbon chains are saturated and others have a small number of unsaturated C=C double bonds. The presence of unsaturated bonds has important implications regarding the thermal stability of the fuels [1], and as discussed below, double bonds also have a strong effect on the kinetics of the fuel ignition and commbustion. The common way of identifying these methyl ester components is to denote the length of the carbon chain (as 'X') and the number of double bonds (as 'Y') in the form of CX:Y. Thus methyl stearate, which has a saturated chain of 18 C atoms with no double bonds is denoted as C18:0 and methyl linoleate is denoted as C18:2, or a carbon chain with 18 C atoms and two double bonds.

The two most commonly used biodiesel fuels are soy oil biodiesel (also called "soy methyl ester" or SME) in the United States and rapeseed oil biodiesel (or "rapeseed methyl ester", RME) in Western Europe. Interestingly, both consist primarily of the same 5 major components, methyl stearate (C18:0), methyl oleate (C18:1), methyl linoleate (C18:2) methyl linolenate (C18:3) and methyl palmitate (C16:0). These components are shown schematically in Fig. 1, showing the close relationship between all 5 of these components. The H atoms are not indicated in this diagram, but there are 3 H atoms where the carbon atom is labeled with a 'p', two H atoms where the carbon is labeled with 's' , 'a', or 's_{co}', and one H atom where the carbon is labeled with 'v'. The notation system CX:Y is not entirely sufficient to describe actual biodiesel fuel components, since in principle there could be many possible locations of the double bond in biofuel component (C18:1), but methyl oleate (C18:1) consistently has the

double bond at the same location at the exact center of the carbon chain, as shown in Fig. 1b. The same consistency is a feature of the other unsaturated methyl esters shown in Fig. 1, and this consistency plays a significant role in development of kinetic reaction mechanisms for these fuel components as described below. The molecular biology of the production of fatty acids in plants and animals is a very active field at the present time, and a good summary of some of this work can be found in Wallis et al. [7]. Based on the fuel components shown here, these 5 components were selected for inclusion in the present study, and they provide a suitable basis for a wide variety of representative kinetic studies of biodiesel fuel.

Table 1 summarizes the approximate fractions of each component in SME and RME, with values taken from the literature, as well as the measured cetane numbers (CN) for each component. Also shown are values of the Derived Cetane Number (DCN), determined by Alexander and Ratcliff [8] using an Ignition Quality Tester (IQT). The precise relationship between the conventional CN, which is measured in a CFR engine under a specific set of conditions, and the DCN, which is measured under somewhat different conditions, has not been established, but for the purposes of this study, both quantities display the same trends. These data will be documented and discussed below, but one important fact is that the relative compositions of species in RME and SME are not the same; the major component of RME is methyl oleate, with only one C=C double bond, while the major component of SME is methyl linoleate, which has two C=C double bonds.

Some other large methyl ester mixtures derived from plant oils have the same components as the fuels modeled in the present study. The same 5 methyl esters are the major constituents of palm oil, jatropha oil, corn oil, cottonseed oil, linseed oil, safflower oil,

sunflower oil, and tallow methyl ester fuels, although each of these fuels has unique fractions of each of the 5 components [1,9]. Although the present study is focused on two particular mixtures of these 5 components in RME and SME, the present kinetic reaction mechanism is equally valid for these other methyl ester fuels, simply by specifying different initial amounts of each of the 5 components as initial conditions for a computation, based on the compositions of the methyl ester fuel to be studied. The general field describing and understanding in fundamental terms the similarities and differences in the molecular compositions of the methyl ester species mixtures derived from different plant oils, animal fats, and algae is rather new, but some of these issues are discussed by Graboske and McCormick [1] and by Wallis et al. [7].

PREVIOUS STUDIES

While engine-based engineering studies of biodiesel fuels have been carried out for some years [1], careful kinetic studies have begun to appear only in the past few years, and this applies equally to laboratory experiments, engine experiments, and to computational studies. This is easily understood by noting that biodiesel fuels consist of rather large molecules. Such molecules have low vapor pressures, making it difficult to carry out gas-phase laboratory experiments in facilities most commonly used for kinetic studies such as shock tubes, flow reactors, stirred reactors and laminar flames. The large number of heavy atoms and the asymmetry of the large methyl ester molecules have made it difficult to build kinetic reaction mechanisms for them until very recently. The sizes of the molecules continue to be too large for most theory techniques, such as electronic structure methods. Fortunately, both laboratory experiments and kinetic models have begun to emerge very recently as these limitations have

found new solutions. In addition, single-cylinder engine studies of combustion of biodiesel fuels are being used [9-12] to evaluate the performance characteristics of these fuels.

Combustion of small methyl and ethyl ester fuels has been studied for some time in spatially homogeneous studies in shock tubes, flow reactors, and rapid compression machines, and also in low pressure premixed laminar flames [13-23]. These studies provide a valuable basis for detailed kinetic reaction mechanisms to simulate the oxidation of the methyl ester moiety combined with a hydrocarbon group.

Very recently, experiments and kinetic modeling studies have begun to appear in which methyl and ethyl esters with much larger hydrocarbon radicals are featured. These studies have examined ignition and combustion of alkyl esters from methyl and ethyl hexanoate and methyl and ethyl heptanoate to methyl decanoate [24-33], followed closely by extensions to methyl stearate and rapeseed methyl ester [34-37].

Several important points have been made regarding the general features of combustion kinetics of large methyl esters. Zhang and Boehman [38] used a motored engine to study combustion of methyl and ethyl octanoates, providing insights into the relative reactivity of different H atoms in the C8 alkyl chains of these molecules, in particular the α-site adjacent to the C=O in the alkyl esters. Dagaut et al. [34] carried out jet-stirred reactor (JSR) experiments using rapeseed methyl ester (RME) fuel, describing the major reaction pathways for oxidation of the major components of RME. No detailed chemical kinetic mechanism was then available specifically for the large methyl ester components, but Dagaut et al. showed that most of the trends observed could be described quite well in terms of a detailed chemical kinetic reaction mechanism for *n*-hexadecane. These computations demonstrated that, for saturated methyl

esters, most of the important combustion properties are extremely similar to those of a saturated alkane fuel without the attached methyl ester group.

Kinetic mechanisms published in 2008 for the saturated methyl ester fuels methyl hexanoate [25] and methyl decanoate [29] demonstrated that detailed kinetic mechanisms for larger methyl esters were possible and could provide the same level of accuracy and detail as past kinetic mechanisms for *iso*-octane, *n*-heptane, and other large alkanes [39-41]. Dayma et al. [25] carried out JSR experiments to validate their own new kinetic mechanism for methyl hexanoate. In contrast, in the absence of available experimental data for methyl decanoate combustion, Herbinet et al. [29] used experiments from related fuels for validation purposes, including shock tube experiments [42,43] using *n*-decane as the fuel, JSR experiments using RME as the fuel [34], and motored engine experiments using mixtures of *n*-heptane and methyl decanoate [10-12]. The similarities in ignition behavior of the saturated species n-decane and methyl decanoate demonstrated that the long saturated straight-chain portions of both fuels were primarily responsible for their rates of ignition, the same conclusion as that reached by Dagaut et al. [34] which compared the combustion of RME with *n*-cetane. The mechanisms for two unsaturated methyl decenoate isomers [30] examined the role of unsaturated C=C double bonds in inhibiting low temperature RO_2 isomerization reactions that had been shown to be important in hydrocarbon alkylperoxy radical isomerization reaction sequences [39,40], finding that carbon double bonds inhibit RO_2 isomerization, consistent with concurrent studies in which the primary fuel was a purely hydrocarbon species with such a carbon double bond [12,44-46].

Hakka et al. [47] examined oxidation of mixtures of *n*-decane and methyl palmitate (at a ratio of 74/26 in the fuel) in a jet-stirred reactor at temperatures from 500K to 1100K,

observing a pronounced NTC region extending from about 600K to 750K, with a conventional reaction region for temperatures above about 800K. Bax et al. [48] reported similar results of JSR experiments for mixtures of *n*-decane and methyl oleate with the same fuel ratio of 74/26, again observing a strong NTC region over the temperature range of 600K to 750K. Thus the two mixtures of *n*-decane with either methyl palmitate or methyl oleate showed very similar reaction behavior under these JSR conditions. Both of these studies were very important because they provided the first laboratory experimental data that could be used for model validation of any of the 5 individual biodiesel components in the present model development study, although neither study included detailed chemical kinetic reaction mechanisms for the methyl ester components in these mixed fuels. Both Hakka et al. and Bax et al. did comment extensively on possible mechanistic explanations for their observations.

Two important reviews have appeared recently, and both are excellent summaries of large bodies of experimental engine studies of biodiesel fuels [49] and a great deal of kinetic modeling literature [50].

MECHANISM DEVELOPMENT

The detailed chemical kinetic reaction mechanism for the present fuel species was assembled by combining several major parts. The first part consists of a "core" mechanism, which involves small molecule submechanisms for species such as H_2, CO, CH_4 and others as large as butane or pentane. For many of the elementary reaction in this core mechanism, rates have been studied experimentally or computed from first-principles electronic structure techniques. For the present study, we have adopted a recent small molecule mechanism of

Curran et al. [51] which itself was built onto an even more basic H_2/O_2 mechanism [52,53]. In addition, since the long straight-chain portions of methyl stearate and methyl palmitate are structurally identical to *n*-alkane molecules of similar length, we have included the *n*-alkane kinetic mechanisms developed recently for *n*-alkanes as large as *n*-hexadecane [41] and have extended those mechanisms to include *n*-$C_{17}H_{36}$ to treat the 1-$C_{17}H_{35}$ *n*-alkyl radical that can be produced from breaking the bond between the methyl ester group in methyl stearate and the long carbon chain containing 17 C atoms. The third part of the present mechanism represents the elementary species, reactions and reaction rates describing the large methyl ester fuels themselves and their oxygenated intermediates produced during oxidation. Unfortunately, for most practical hydrocarbon and related fuels, and particularly for these large alkyl ester fuel species, site-specific, temperature dependent reaction rates have not been measured or computed, so the rates of most reactions of such fuels must be estimated. To facilitate those estimates, we have built on the recent studies of smaller methyl esters noted above, which have established that H atom abstraction reactions depend mostly on the type (i.e., primary, secondary, tertiary, allylic, vinylic) of C-H bond is being broken. Rates of radical decomposition via β-scission, additions of molecular O_2 to alkyl radicals, rates of alkylperoxy radical isomerizations, and many other reactions of the methyl alkylperoxy radical isomerizations have been estimated based on past experience [39-41,51], with alkylperoxy systems.

In previous detailed chemical kinetic reaction mechanisms for the large hydrocarbon fuels *n*-heptane [39] and *iso*-octane [40], we identified 25 different classes of elementary reactions generally believed to play a role in the oxidation of such fuels. Using reaction rates most often measured or estimated for similar reactions in much smaller hydrocarbon

molecules, we assigned similar rates expressions and product distributions to the same reactions in the larger fuel molecules. Such an estimation process involves uncertainties, and better rate expressions would be valuable in refining these reaction mechanisms. At the same time, sensitivity analyses of these rate expressions have not shown unusually great sensitivities to most of these reaction rate expressions. In addition, computed results using these estimated rate expressions have led to reliable computed predictions of combustion rates for these fuels, so we have continued to use this technique for other classes of hydrocarbon fuels [41,54,55]. The same general approach is used by Battin-Leclerc et al. [27,28,56-58] who use the EXGAS software to automatically generate new detailed chemical kinetic reaction mechanisms for other large hydrocarbon and other fuels, with similarly good results. Until high quality theoretical techniques become able to compute reaction rates of elementary reactions of large hydrocarbon species, this estimation technique will continue to be used extensively.

Early kinetic modeling studies of methyl butanoate [14-16] established many reaction pathways and reaction rates describing oxidation of the methyl ester group, and subsequent kinetic modeling work for other small alkyl esters [22] refined these methyl ester mechanisms. Herbinet et al. [29] extended the same approach to describe combustion of methyl decanoate, and Dayma et al. [25,26] employed the same type of extension of methyl butanoate mechanism to larger methyl ester fuels. Herbinet et al. [30] then examined the importance of C=C double bonds within the methyl decanoate structure and proposed mechanistic techniques to describe the kinetic features introduced by these double bonds, leading to detailed chemical kinetic reaction mechanisms for two distinct isomers of methyl decenoate. In particular, Herbinet et al. concluded that C=C double bonds within the straight-chain carbon portion of methyl

decenoate inhibited intramolecular H atom abstraction reactions that are important processes for low temperature oxidation and ignition of saturated hydrocarbons. This role of C=C double bonds in a straight chain was observed previously in isomers of hexene [44-46] and described kinetically in modeling analysis of Mehl et al. [44] and Bounaceur et al. [46], so the inhibition of low temperature reactivity of methyl decenoate relative to methyl decanoate by Herbinet et al. is very consistent with the behavior of other fuels. This observation is a central issue in the kinetics of the present fuels, since methyl stearate, methyl oleate, methyl linoleate and methyl linolenate differ structurally only by the introduction of C=C double bonds into methyl stearate.

In the present modeling study, we have adopted most of the kinetic features developed by Herbinet et al. [29,30], appropriately extended to the significantly longer C chains in methyl stearate and methyl palmitate, and we have employed the same approach of Herbinet et al. and Mehl et al. [44] to describe the influences of the C=C double bonds. The results of the additional C=C double bonds in methyl linoleate and methyl linolenate are described below.

Curran et al. [39,40] used an approach of defining 25 reaction classes that describe most of the kinetic functions that are important in hydrocarbon oxidation reaction mechanisms. We have followed Herbinet et al. [30] by using the same reaction classes, but with modifications as needed for the special conditions of the species in this biodiesel fuel mixture. Because of these methyl ester components, there are a significant number of new types of reactions, or at least new conditions for existing reaction classes. It is those new features that are responsible for the differences in combustion behavior between each of the five major fuel components. For example, as seen in Table 1, the cetane number (CN) of the major saturated species methyl stearate is approximately 101, while the corresponding methyl ester with one double C=C bond

(methyl oleate) has a CN = 59, methyl linoleate with two C=C double bonds has a CN = 38, and methyl linolenate with three C=C double bonds has a CN = 23. Since the 4 molecules have the same size and structure, except for the presence of C=C double bonds in the carbon chain, those differences in reactivity, most notably in the low temperature regime, must be due to the kinetics and thermochemistry involving the double bonds.

REACTION CLASSES

The high temperature submechanisms for the five biodiesel components are the same as those used previously for other types of fuels, consisting of:

1. Fuel unimolecular decomposition
2. H atom abstraction from the fuel
3. Alkyl and ester alkyl radical decomposition
4. Alkyl and ester alkyl radical + O_2 to produce alkene and HO_2 directly
5. Alkyl and ester alkyl radical isomerization
6. Abstraction reactions from alkenes by OH, H, O, and CH_3.
7. Addition of radical species to alkenes
8. Alkenyl radical decomposition
9. Alkene decomposition

Since three of the biodiesel components have one or more double C=C bonds, these reaction classes must be generalized somewhat to include these unsaturated fuel species, and the term "alkyl" radical has been extended to include alkyl and similar radicals (i.e., alkyl ester)

containing a methyl ester group. We discuss these issues briefly and refer the reader to Herbinet et al. [29,30] for further details.

For each of the five fuel components, the fuel is assumed to decompose primarily by breaking C-C bonds. For the three fuels containing one or more C=C double bonds, no unimolecular decomposition was included that involved breaking any of the double bonds. In the methyl ester group, initiation can occur by breaking either of the C-O bonds or by breaking the C-(CO) bond, although as noted by Osmont et al. [59], these bonds are stronger than the C-C bonds in the long chain. We have written all of these reactions in the exothermic addition direction, so the decomposition rates are then computed from the recombination reaction rates and microscopic reversibility. In addition, for the unsaturated fuel species, molecular reactions such as retroene decompositions are included, using the approach of Metcalfe et al. [15] as implemented by Herbinet et al. [30]. For the saturated and unsaturated fuel components, molecular elimination producing methyl ethanoate and a stable unsaturated hydrocarbon chain was also included, again following Herbinet et al. [29,30].

Abstraction of H atoms from each fuel molecule depends on the type of abstracting radical species and on the C-H bond energy of the H atom being abstracted. In Fig. 1, the types of C-H bonds at each site are identified. The C-H bond (S_{CO} in Fig. 1) at the site adjacent to the methyl ester group is relatively weak, and we use abstraction rates adopted from those from tertiary C-H sites in other molecules. The C-H bonds in both terminal methyl groups are assumed to be equal to those in conventional primary C-H sites. The remainder are conventional primary and secondary C-H sites, as well as conventional allylic and vinylic C-H

bonds associated with the C=C double bonds. All of these rates are tabulated in Herbinet et al. [27,30] or Curran [60].

Diagrams of methyl stearate, methyl oleate, methyl linoleate and methyl linolenate are shown in Fig. 1, where the methyl ester group is at the right side of each molecule diagram. The type of C-H bond at each C site is illustrated by the letter (p, s, a, v, and s_{co} for primary, secondary, allyl, vinyl, and the weakened secondary bond described in the previous paragraph), and each C is labeled to illustrate the numbering system used in the kinetic reaction mechanism.

Alkyl and ester alkyl decomposition reactions are primarily β-scission reactions of the radicals produced from H atom abstraction reactions from each of the fuel species, primarily breaking C-C bonds. Such reactions generally produce a smaller hydrocarbon radical and another species with a new C=C double bond. We also include β-scission reactions that break a C-H bond, producing an H atom product and a new C=C double bond. These reactions are written in the exothermic, addition direction, with the decomposition rates calculated from the addition rate and microscopic reversibility. All of the reaction rates for these decomposition reactions follow the same rules as in Herbinet et al. [29,30]. Due to the presence of numerous C=C bonds in three of the fuel components, abstraction of an allylic H atom produces mesomeric,resonantly stabilized pairs of radicals, each of which is considered in subsequent reactions, as described by Herbinet et al. [30]. Waddington reaction sequences, in which an olefin adds OH at a double bond, followed by O_2 addition and internal isomerization, were included in the reaction mechanisms for the unsaturated methyl ester fuel components but were not found to be significant in contributing to fuel consumption.

Alkyl and ester alkyl radical isomerization reactions follow the rate rules developed in the past for purely hydrocarbon fuel molecules. The rates of these reactions are determined from the number of atoms in the transition state ring which is responsible for the internal abstraction and by the strength of the C-H bond being broken, as described in previous mechanisms [29,30,39,40]. However, in some of the present fuels, the H atom being abstracted can be located at a vinylic site, so the activation energy for that internal abstraction is increased by 15 kcal/mol to reflect that stronger C-H bond, making such isomerization reactions relatively quite slow.

In previous kinetic mechanisms [29,39-41,55] for saturated hydrocarbon species, the submechanisms for the oxidation of the conjugate olefin species were lumped, reflecting the fact that the concentrations of these olefin species were expected to be rather small. However, the present mechanism must take into account that methyl oleate is one of 16 olefins that can be produced from methyl stearate, so we must at least treat methyl oleate with a site-specific reaction mechanism, since methyl oleate will be present as a major component of the biodiesel fuel. Similarly, oxidation of methyl oleate leads to methyl linoleate as one of 15 di-olefins that can be produced. Again, since methyl linoleate is a major component in SME and RME biodiesel fuels, its concentration will be relatively large and its consumption should be treated in considerable detail, particularly including site-specific H atom abstraction reactions and subsequent low temperature reaction sequences. The same principle applies to methyl linolenate, which is one of 14 tri-olefins that can be produced from methyl linoleate. Thus, in the present mechanism, we have chosen to include accurate, detailed site-specific reaction rates for methyl oleate, methyl linoleate, and methyl linolenate, but the other 15 olefins, 14 di-

olefins and 13 tri-olefins are treated as lumped species, in the same way that we treated alkene and alkenyl radicals in reaction classes 6-9 in past mechanisms for saturated hydrocarbon fuels. Also note that there are a multitude of other di-olefin species not based on methyl oleate and tri-olefin species not based on methyl linoleate that are possible in these fuels that are treated as lumped species.

In the case of olefin species from methyl stearate, methyl oleate is modeled as a primary fuel species, with reactions from Classes 1-5 as summarized above, but with some of the C-H bonds consisting of abstractions from allylic and vinylic sites, decompositions that vary depending on the location of the double bond in methyl oleate, and isomerization reactions of the methyl oleate radicals that depend on the location of the double bond. All of the other olefin species from methyl stearate are treated in lumped fashion.

Herbinet et al. [30] note that abstraction of an H atom from an allylic site in methyl oleate results in a resonantly stabilized radical. For example, abstraction of an H atom from the 8-site in methyl oleate produces the mod9d8j radical species, which is resonantly equivalent to the mod8d10j radical. This leads then to two possible C-C bonds that can be broken by β-scission of this radical, one by breaking the #6 C-C bond in mod9d8j to produce mh6j and 1,3-$C_{12}H_{22}$, a hydrocarbon di-olefin species, or by breaking the #11 C-C bond in its resonantly stabilized isomer mod8d10j to produce a methyl ester di-olefin species mu8d10d and the alkyl radical 1-C_7H_{15}. The possibilities grow as the number of double bonds increase in methyl linoleate and methyl linolenate, and these are all included in the present mechanisms.

For the lumped olefins, di-olefins and tri-olefins with methyl ester groups included, each species is assumed to react via H atom abstraction reactions with H, O, OH, HO_2, CH_3, CH_3O,

CH_3O_2, C_2H_3, C_2H_5, and O_2, producing a single lumped radical that is then assumed to decompose to smaller species and eventually to small, usually unsaturated radicals in the C_1 - C_4 core kinetic mechanism. For example, the mod2d9d di-olefin is consumed by these H atom abstraction reactions to produce the mod9dxdj radical, and the mod3d9d, mod4d9d and most other related di-olefins also produce the same lumped radical mod9dxdj. However, the mod9d12d di-olefin, which is methyl linoleate, is consumed by site-specific H atom abstractions that produce site-specific radicals including mod9d12d2j, mod9d12d3j, mod9d12d4j and all the others to mod9d12d18j. Each of these di-olefin radicals then can decompose via β-scission to unique products depending on the structure of the di-olefin radical. The same logic applies to the many lumped tri-olefin species mod9d12dxxd except for the specific tri-olefin mod9d12d15d, which is methyl linolenate and is treated in a site-specific manner.

LOW TEMPERATURE MECHANISMS

For the most part, low temperature oxidation reaction pathways encountered in alkane fuels are the same for methyl ester fuels. Curran et al. [39,40] divided the low temperature mechanism into 16 distinct reaction classes, as well as a variety of other miscellaneous steps, most of which we have adopted without changes, just as Herbinet et al. [29,30] constructed their mechanisms via the same reaction classes. The most important low temperature reaction classes involve alkylperoxy radical isomerization pathways [61] that begin with the addition of molecular oxygen to alkyl-like radicals, followed by isomerization of the resulting alkylperoxy and esteralkylperoxy (RO_2) radicals to produce hydroperoxyalkyl radicals. These and subsequent reaction sequences of low temperature oxidation occur at rates that are very

similar to the analogous reactions that are now familiar in low temperature hydrocarbon kinetics [29,30,39,40].

The presence of a methyl ester group in all of these fuel molecules and the presence of C=C double bonds in some of them modify the rates of some of the specific reactions. These modifications have been explored in detail in past kinetic studies of methyl ester fuels [25-30] and hydrocarbon fuels containing C=C double bonds [44-46], and the present mechanism combines both of these features as needed for each fuel component. In particular, internal abstraction of an H atom at an allylic site is assumed to have the same A factor as internal abstraction from a conventional site, but with a reduced activation energy due to the weaker C-H bond being broken. Following Mehl et al. [44] and Bounaceur et al. [46], we have assumed that RO_2 and O_2QOH isomerizations do not proceed if a double bond is contained within the transition state ring for the reaction. In the mechanism of Herbinet et al. [30] for methyl decenoate, the double bond was assumed to contribute an additional 15 kcal/mol to the energy barrier for these isomerization reactions, and we have simply extended this barrier to a level where the reactions cannot take place at any practical rate. This class of isomerization reaction, and the degree of interaction of the RO_2 group with the imbedded C=C double bond, needs further attention from both theoretical and direct experimental studies.

The resulting reaction mechanism contains more than 4800 chemical species and nearly 20,000 elementary chemical reactions. The thermochemical data file and the detailed chemical kinetic reaction mechanism are available on our web page at
https://www-pls.llnl.gov/?url=science_and_technology-chemistry-combustion
and this includes the species and bond location naming system being used.

MODEL VALIDATIONS

There are only a few laboratory-scale experiments that provide data that can be used to test chemical kinetic reaction mechanisms for biodiesel fuel and its components, all of which have begun to appear in the past few years. In addition, existing biodiesel fuels and their individual components have been tested to determine their cetane numbers for diesel ignition. We have used as much as possible of this available kinetic literature to attempt to validate the present kinetic mechanisms, for the individual methyl ester components and for the composite biodiesel fuels. In addition, we have carried out some purely numerical "experiments" to compare the combustion properties of the biodiesel components and mixtures with other hydrocarbon species that are commonly found in diesel fuels. We begin with the simulations of the experiments in which one specific component of the biodiesel fuel was studied. At the same time, it is very clear that more systematic kinetics experiments are needed to refine existing models, especially the present 5-component mechanism.

Hakka et al. [47] studied the oxidation of a mixture of 26% methyl palmitate/74% *n*-decane, a second mixture of 26% *n*-hexadecane/74% *n*-decane, and a third case where the fuel was entirely *n*-decane. In each case, the total fuel mole fraction was 0.002. All three experiments were carried out at atmospheric pressure for stoichiometric fuel/O_2 mixtures, highly dilute in helium. A temperature range from 550K to 1100K was examined, and the residence time in the JSR was 1.5s. In all three experiments, the overall reaction revealed two separate regions of high reactivity. The first reactive period occurs at JSR temperatures between 500K and 700K, rising to a maximum conversion of approximately 60% at 650K, then falling close to zero at about 775K, then increasing again above about 800K to a final value of

100% fuel conversion at higher temperatures. For the mixture of *n*-decane and methyl palmitate, Hakka et al. reported that the overall reactivity of the mixture of the two fuel components showed the same two ranges of considerable reactivity, shown by the fractional conversion of the two fuel components in Fig. 2.

We have used the Chemkin software package [62] to simulate these JSR experiments, and our kinetic model shows results that are very similar to the experimental results. Both the experiments and computed results show a slightly greater conversion of the methyl palmitate than the *n*-decane in the low temperature reaction region, while the two fuel conversions are nearly equal in the higher temperature range. The two distinct reaction regimes are shown very strongly in both the experimental and computational results, and the agreement between the experimental and computational results is excellent. The slightly greater amount of low temperature conversion of methyl palmitate than that of *n*-decane can be attributed primarily to the weakly bound H atoms at the '2' site adjacent to the methyl ester group in methyl palmitate [28-30,36,37], so the total rate of methyl palmitate consumption is slightly greater than that of *n*-decane.

The primary reaction intermediates such as CO, CO_2, CH_4, and CH_3OH show very good agreement between experiment and modeling results. Comparisons between computed and experimentally measured intermediate species mole fractions are shown in Figures 3 and 4. Fig. 3 shows comparisons for some of the major 1-alkenes, all of which show evidence of the low temperature reaction regime as well as the higher temperature reactivity. Details of the kinetic results show that these 1-olefins are produced both by the *n*-decane fuel component

and by the methyl palmitate component. The peak concentrations of these olefins decrease steadily as their sizes increase, from 60 ppm for 1-heptene to about 3 ppm for 1-tridecene.

Figure 4 shows the computed and experimental levels of some of the unsaturated methyl ester intermediate species, specifically the methyl ester (1-olefin methyl ester) in which the double bond is located at the end farthest from the methyl ester group. Both 1-olefins and unsaturated 1-olefin methyl esters are direct products of β-scission following the abstraction of an H atom in the saturated linear chain in methyl palmitate. For example, if an H atom is abstracted at the '11' location in the linear carbon chain (see Figure 1), then there are two major β-scission reactions of the resulting mhd11j radical. These would be:

mhd11j = mn9j + $1C_7H_{14}$

mhd11j = med11d + pC_4H_9

Thus this specific abstraction reaction produces stable intermediates $1C_7H_{14}$ and med11d (11-dodecene methyl ester), and these are both major products of this reaction as seen in Figures 3 and 4.

It is interesting to note that the 1-olefin concentrations are significantly higher than their corresponding 1-olefin methyl esters. Since all of them are produced by decomposition of H atom abstraction reactions, one should expect a general ratio of 3:1 of 1-olefins:1-olefin methyl esters, if the initial concentrations of the *n*-alkane and the saturated methyl ester were equal. That is, each abstraction from the *n*-alkane would produce approximately 2 olefins, while each saturated methyl ester should produce one 1-olefin and one 1-olefin methyl ester. The observed ratios of these species types are roughly consistent with the initial fuel composition.

Overall, the present mechanism produces agreement with experimental results of Hakka et al. [47] that is very similar to the agreement provided by Herbinet et al. [36]. The paper of Herbinet et al. provides an excellent and extensive analysis of these experiments of Hakka et al. The present mechanism shows a slightly greater low temperature selectivity for unsaturated methyl esters than the model of Herbinet et al., but these minor differences are due to small differences in reaction rate rules for the low temperature reaction classes. Both models are based largely on the past work of Herbinet et al. [29] and both provide a reliable submechanism for methyl palmitate over the entire temperature range of the experiments.

Bax et al. [48] repeated the same JSR experiments as those of Hakka et al. [47], replacing the methyl palmitate with an equal initial mole fraction of methyl oleate, again mixed with 74% *n*-decane, for a total fuel mole fraction of 0.002. They presented their results for their *n*-decane/methyl oleate mixture, combining them with the measurements from Hakka et al. in order to describe the differences between a saturated methyl ester and another methyl ester with one C=C double bond. This double bond, shown schematically in Fig. 1, is located in the middle of the C_{18} straight chain. The results of Bax et al. show fuel component conversions for the *n*-decane/methyl oleate mixtures that are very close to those of the *n*-decane/methyl palmitate mixtures. Experimental levels of major intermediate species produced by the two fuel mixtures were also quite similar to those in the *n*-decane/methyl palmitate mixture, but in the high temperature regime, oxidation of the methyl oleate mixture was found to be slightly faster than the mixture with methyl palmitate.

Our computed results for the *n*-decane/methyl oleate mixture show good agreement with experimental values of Bax et al. The computed and experimental values for conversion of

methyl oleate and *n*-decane are shown in Fig. 5, with somewhat greater conversion at lower temperatures for methyl oleate than for *n*-decane in these mixtures. It is important to note that these values represent simple consumption of the two fuel molecules, not overall rate of oxidation, and the most significant difference between methyl oleate and *n*-decane is the fact that methyl oleate has 6 H atoms with C-H bond strengths that are significantly lower than those in *n*-decane. These weakly bound, easily abstracted H atoms are the two H atoms bonded at the C atom adjacent to the methyl ester, as well as 4 H atoms bonded at allylic sites in methyl oleate, due to the presence of the centrally located double bond.

Comparisons between experimentally measured and computed species profiles for the major intermediates are shown in Fig. 6. Overall agreement for these and other major species are good, indicating that the main features of the oxidation are being reproduced accurately.

Similar to the case above with methyl palmitate, model results for the *n*-decane/methyl oleate mixtures produce significant levels of species that are produced from β-scission of the radicals formed from H atom abstraction from the fuel. Many of those species produced from *n*-decane are the same as those also seen in the *n*-decane/methyl palmitate experiments of Hakka et al. [47], which is sensible since *n*-decane provides 74% of the fuel in both fuel mixtures. However, the presence of the double bond in the middle of the methyl oleate molecule leads to a wide range of stable products with two double bonds that are not observed in the results of Hakka et al.. Bax et al. describe a variety of mechanisms that can lead to large hydrocarbon diene species, with one of the double bonds representing the initial double bond imbedded in the oleate fuel species, as well as a second double bond resulting from the β-

scission of the alkenyl ester radical. Bax et al. also describe a wide variety of methyl ester diene species, which have the same formation pathways as the hydrocarbon diene intermediates.

Bax et al. did not report a lengthy list or extensive figures with concentrations of these hydrocarbon and methyl ester diene species, instead emphasizing a smaller number of illustrative examples, but our model calculations are consistent with their analysis and some of the main species they plot also appear in our computed results as significant products. We did observe one interesting point that should have implications for future refinements and related model developments. For fuel species that are large and have complex structures, and methyl oleate has both properties, there are many opportunities in kinetic mechanisms for multiple reaction pathways to occur, and it is quite possible to produce an accurate prediction of some integrated property such as an ignition delay time, burning velocity, or overall rate of reaction, and still not describe the complete details of the reaction. This is particularly true in the low temperature regime, where a combination of resonantly stabilized radicals, complex decompositions of oxygenated radicals where as many as 5 or 6 possible reaction pathways are possible, and multiple pathways for large radical isomerization are possible, all make it extremely challenging to identify all of the elementary reactions that can occur. Experience has demonstrated that, in most cases, the most important feature is the impact that these choices make on the chain branching and propagation rates of the reaction, which will affect the integrated variable that is being predicted, so that often the choice of specific reaction pathways makes little difference. However, when the species concentrations of selected intermediates are used to test the mechanism, the details of the mechanism may appear faulty. For the purposes of the present model development effort, we place particular value on the

very good agreement between the overall reactivity and the major species concentrations, which are predicted well.

The third set of mechanism validation results is the experimental JSR study of Dagaut et al. [34] in which rapeseed methyl ester (RME) was used as the fuel. Three mixtures were studied at atmospheric pressure and a residence time of 0.07s, at equivalence ratios of 0.25, 0.5, and 1.0, and a fourth mixture at atmospheric pressure, a residence time of 0.1s and an equivalence ratio of 1.5. Two additional experiments were carried out at 10 atm pressure and a residence time of 1s for equivalence ratios of 0.5 and 1.0. The atmospheric pressure mixtures were studied for operating temperatures from 900K to 1400K, and the 10 bar experiments were studied for temperatures from 800K to about 1200K. Each experiment used a low initial RME concentration (0.05% fuel), with the initial O_2 required for the given equivalence ratio, and a high degree of dilution by N_2. Dagaut et al. carried out kinetic model simulations using *n*-hexadecane as a surrogate for RME, and their *n*-hexadecane model showed a good degree of agreement between the model and experiments for a large number of intermediate and final product species. As noted earlier, those results have significant implications with respect to definition of useful surrogates for complex fuels.

Biodiesel fuel is different from conventional diesel fuel in that common diesel fuel contains many hundreds of individual hydrocarbon species, while biodiesel fuel contains a small number of unique, repeatable components. Dagaut et al. [34] described their RME fuel as "a complex mixture of C_{14} - C_{22} esters with highly saturated carbon chain. The composition of the fuel was 0.1% C_{14}, 5.4% C_{16}, 92.0% C_{18}, 2.0%C_{20} and 0.5% C_{22}, with mostly one double bond on the acid chain." Schönborn et al. [9] list similar but not exactly the same fractions, and Van

Gerpen et al. [63] from the US National Renewable Energy Laboratory reported C16:0 (4.3%), C18:0 (1.3%), C18:1 (59.9%), C18:2 (21.1%) and C18:3 (13.2%). We have used these values from Van Gerpen et al. for our RME surrogate to simulate the experimental results of Dagaut et al. and other RME and SME simulations below, and they are the values used in Table 1 above.

Each of the Dagaut et al. experiments was simulated using the present reaction mechanism for the 5-component mixture representing RME. The overall agreement between computed results and experimental values was generally satisfactory, with all of the major trends reproduced well, but with agreement for individual species profiles varying from very good to marginal. Using the stoichiometric mixture experiments at 10 bar pressure for illustration, some of the major species are shown in Fig. 7a and the major olefin species are shown in Fig. 7b, showing generally good agreement. Experimental results are shown as symbols, computed results as solid lines. However, in some specific examples, the agreement is not particularly good. For example, in the stoichiometric mixture at 10 atm shown in Fig. 7a, the computed and experimental CO and CO_2 values both agree fairly well, but the values for H_2 do not agree as well, with the experimental values continuing to increase with increasing JSR temperature, while the computed results reach a maximum value at about 950K, and then decrease steadily. Since this example is at stoichiometric fuel/oxygen conditions, the H_2 should be expected to decrease eventually, but the experimental results provided here indicate that the H_2 has not reached its maximum value at 1150K.

Most H_2 consumption is due to reaction with OH to produce H_2O + H, but the reaction rate of OH with most hydrocarbon species is larger than its rate of reaction with H_2, so the presence of significant levels of hydrocarbon will keep the OH level too low to consume much

of the H_2. The same is true of CO, which also is oxidized primarily by reaction with OH, and its rate of reaction with OH is also smaller than the rate of OH with most hydrocarbons. Once all or most of the remaining hydrocarbon species have been consumed, the H_2 and CO are rapidly consumed. As seen in Fig. 7b, the computed level of C_2H_4 is lower than that found in the experiments by about a factor of two, so the computed OH level is probably higher than that of the experiments, resulting in a more rapid consumption of H_2 in the computed results. It is a bit odd that the CO is being consumed quite rapidly from 1000K to 1150K in the experiments while the H_2 level continues to increase over this temperature interval. Under most conditions, the CO and H_2 consumption tend to follow somewhat parallel curves, so this difference between the computed and measured H_2 results merits further study.

The trends in levels of 1-olefins seen experimentally are reproduced quite well by the model, decreasing steadily as the size of the 1-olefin increases. However, the computations show that the 1-butene level computed by the model is a bit lower than in the experiments, and a modest inversion is computed in the relative levels of 1-butene and 1-pentene. This inversion may be due to minor errors in the assumed product distributions of the low temperature kinetic reaction pathways for these large methyl ester fuels. Further study of these product distributions is needed.

Computational extensions of the operating temperature of the experiments of Dagaut et al. to temperatures lower than those examined experimentally, specifically to 500K, showed no NTC behavior or low temperature reaction activity in the atmospheric pressure experiments of Dagaut et al. However, similar computational extensions to lower operating temperatures for the Dagaut et al. experiments at 10 bar pressure showed a modest low temperature

reaction region, extending to about 550K. Computed results at these lower temperatures can be seen in Fig.7, including the computed fractional fuel conversion for methyl oleate and methyl palmitate shown in Fig. 7c, showing the low temperature oxidation and slight NTC behavior quite clearly. The computations at 10 bar and an equivalence ratio of 0.5 showed a smaller but still noticeable amount of low temperature reactivity.

Even with the computed low temperature reactivity at 10 bar, the results of Dagaut et al. [34] and the model calculations indicated that RME oxidation at these conditions is in contrast with the JSR experiments of Hakka et al. [47] and Bax et al. [48], which showed extensive levels of low temperature reaction as low as 500K. The lower fuel concentrations of Dagaut et al. (0.05% fuel compared with 0.2% fuel in the Hakka et al. and Bax et al. studies), the shorter residence times of Dagaut et al. (0.07s compared to 1.5s), and the higher heat capacity of the N_2 diluent used by Dagaut et al. compared with He in the Hakka et al. and Bax et al. experiments, all combine to make the low temperature reaction much less prominent in the Dagaut et al. experiments.

The experiments of Dagaut et al. [34] provide valuable data for testing biodiesel fuel kinetics, in particular since there are so few careful kinetic experiments in the literature. As we will discuss below, there is good reason to believe that low temperature fuel reactivity plays a significant role in diesel fuel ignition that is reflected in the cetane number of such fuels. The absence of detectable low temperature reactivity at the conditions in most of the Dagaut et al. RME experiments is unfortunate because it limits our ability to use the experiments to test the low temperature portions of the reaction mechanism. This illustrates well that one valuable application of a kinetic model is to provide guidance when planning an experimental program,

to be sure that important features will be examined if possible. Of course, it is also important in these experiments to limit their exothermicity, so in some conditions it may not be practical to address some issues of interest. The most significant achievement of the work of Dagaut et al. was to demonstrate the ability of an alkane kinetic mechanism, specifically for n-hexadecane, to reproduce so much of the intermediate and high temperature reactivity of RME.

NUMERICAL EXPERIMENTS

In the absence of a more extended body of validation data for these fuels, we have carried out two series of numerical experiments under conditions that have been studied rather extensively for other types of fuels. We then use the computed results to demonstrate the capabilities of this kinetic mechanism, and some of the computed results suggest that the mechanisms have some of the important features of combustion of biodiesel fuels that could be valuable.

JET-STIRRED REACTOR SIMULATION

For the first tests, each of the 5 biodiesel component fuels in Fig. 1 was examined in the JSR under the same experimental conditions as those used by Hakka et al. [47] and Bax et al. [48], except that for these new simulations, the fuel consists of a single methyl ester with no accompanying *n*-decane. For each simulation, a stoichiometric fuel/O_2 mixture was used with 0.2% fuel, diluted by helium, at atmospheric pressure and a residence time of 1.5s.

Each fuel component responded somewhat differently under these conditions, as shown in Fig. 8. The two saturated methyl esters, methyl stearate and methyl palmitate, show

very similar behavior, with a pronounced low temperature reaction zone extending to about 70% fuel consumption. The only small difference between these fuels can be seen at the minimum values for each curve at about 750K, where the methyl palmitate shows slightly less conversion at this point. The methyl ester with one double bond, methyl oleate, shows somewhat less low temperature reactivity than the saturated fuels, but still considerable reactivity, including somewhat more fuel conversion than either methyl stearate or methyl palmitate for temperatures above 700K.

The two remaining components, methyl linoleate with two double bonds, and methyl linolenate with three double bonds, show significantly different behavior from the first three components. Methyl linoleate shows relatively little low temperature reactivity, with a small NTC region at 700K, while methyl linolenate shows even less low temperature reactivity, with a small amount of reaction near 700K but no NTC behavior under these conditions.

It is interesting to compare the results of these calculations with the known cetane numbers for each of these individual fuels. Using values from Table 1 taken from Knothe [49] for cetane numbers, methyl stearate has a CN=101, methyl palmitate has CN=86, methyl oleate has CN=59, methyl linoleate has CN=38, and methyl linoleate has CN=23. The correlation between the low temperature reactivity and cetane number is striking. Boehman et al. [10] emphasized the correlation of ignition delay and autoignition behavior of diesel and surrogate diesel fuels, and Stein et al. [64] related ignition delay with CN, and those results and the present kinetic analyses show clearly that low temperature reactivity, ignition delay, autoigntion and cetane numbers are all intimately connected. That is, fuels with greater amounts of low temperature reactivity and heat release have shorter ignition delays and

therefore ignite earlier and have higher cetane numbers than fuels that have less low temperature reactivity. Of course, cetane number depends on additional factors as well as ignition delay time, but the trend of cetane number increasing in roughly the same manner as the amount of low temperature reactivity is significant.

We then combined the 5 biodiesel components into two different mixtures, one representing the nominal composition approximating the composition of RME and the other representing the nominal composition of SME, using the fractions listed in Table 1. New JSR calculations were carried out for these two surrogate biodiesel blended fuels at the same operating conditions as for the 5 individual fuels and for the Hakka et al. and the Bax et al. experiments. The results of these two computed histories are shown in Fig. 9. There are two important features of these results. First, all five components can be seen to react together, rather than sequentially, but at rather different overall rates for the RME and SME mixtures. This means that, for each fuel mixture, the more reactive components produce radicals that are then used by the less reactive components, producing a sort of "average" behavior for the mixture. The net low temperature reactivity of the RME biodiesel mixture is significantly greater than that of the SME mixture, suggesting that RME biodiesel should be expected, on the basis of these computations, to have a higher CN than the SME biodiesel fuel. While the data are sometimes confusing, most sources indicate that the CN for SME fuel is about 47 and about 54 for the RME fuel [65]. Graboski and McCormick [1] average a large group of values determined for both biodiesel fuels to arrive at an average CN for SME biodiesel of 51 and 53 CN for RME biodiesel. Both results are generally consistent in attributing RME fuel with a larger CN than SME fuel, and the relative amounts of low temperature reactivity shown in Fig. 9

certainly show more low temperature reactivity for RME fuel. Experimental JSR studies for the 5 methyl ester components in these fuels, corresponding to the results of Fig. 8, and direct comparisons in a common facility of the different types of biodiesel fuel would be valuable to confirm this set of predictions and the correlations between ignition in a laboratory facility and the CN.

The computed results in Fig. 9 show quite strongly that RME is more reactive than SME, with considerably more low temperature reactivity. The results for the individual components in Fig. 8 provide the explanation for the differences in the composite fuels. From Table 1 we noted that the most prevalent component in RME is methyl oleate, while the corresponding major component in SME is methyl linoleate. Fig. 8 shows that the oleate is considerably more reactive in the low temperature regime than the linoleate, which provides more low temperature reactivity and a higher CN for RME than for SME.

HOMOGENEOUS AUTOIGNITION OF BIODIESEL FUELS

The intermediate temperature (700K - 1100K) autoignition of hydrocarbon fuels has been used widely to test chemical kinetic reaction mechanisms for many fuels. The original source of this class of problems was the series of shock tube experiments carried out by Adomeit and colleagues. In these studies, ignition of *n*-heptane, *n*-decane, and *iso*-octane [43,66,67] was studied, showing very clearly a region of negative temperature coefficient (NTC) of reaction, with the amount of NTC behavior depending on the molecular structure of the fuel, as well as on equivalence ratio and pressure. Subsequently, the same test conditions have been used to test reaction mechanisms for many other fuels [37,39-41,55,57,58], and further

experiments have been carried out to compare the intermediate temperature ignition of other fuels [54]. Part of the value of such experiments and kinetic modeling is the fact that *n*-heptane and *iso*-octane are primary reference fuels (PRF) for octane ratings of automotive fuels, and it has been interesting to use these shock tube experiments and simulations to relate other fuels to the PRF references. In particular, the relative reactivity of different fuels in the NTC region can be used to provide insights into the octane and cetane ratings of different fuels [55].

Therefore, as another test of the present biodiesel fuel species kinetic models, we carried out autoignition simulations for each single-component methyl ester fuel component, one at a time, for stoichiometric mixtures of each single-component methyl ester fuel in air under the same conditions as those studied by the Adomeit group, specifically at 13.5 bar pressure, assuming reflected shock wave conditions. The results of these calculations are summarized as lines in Fig. 10. Each line represents the ignition delay for one of the methyl ester components from Fig. 1. All five methyl esters have nearly equal ignition delay times at high temperatures, differing primarily at temperatures below about 900K. The two saturated species, methyl stearate and methyl palmitate, have nearly identical ignition delay times over the entire temperature range, including in the NTC regime. For comparison, we have plotted the experimental results for *n*-heptane ignition reported by Ciezki et al. [66] at the same shock tube conditions, and the methyl palmitate and methyl stearate results are similar to the *n*-heptane values over the entire temperature range. The ignition delay times for the next two components, methyl oleate and methyl linoleate, are quite close together in Fig. 10, with the oleate slightly faster to ignite, and the slowest to ignite is methyl linolenate.

As discussed above for the single-component JSR simulations, the ignition delay times of the 5 individual methyl ester fuel components in the NTC region align in the same order as their cetane numbers. The two saturated methyl esters have cetane numbers of 101 and 86, methyl oleate and methyl linoleate have cetane numbers of 59 and 38, and methyl linolenate has a cetane number of 23.

We again used the simulated 5-component RME and SME simulant mixtures as defined above to carry out the same ignition delay calculations as the individual fuels, and these results are indicated as symbols in Fig. 10. These computed values for RME and SME biodiesel are very nearly identical with each other and are very similar to the computed results for methyl oleate and methyl linoleate. The similarities of the biodiesel mixtures to the single component fuels methyl oleate and methyl linoleate are not surprising, since both RME and SME biodiesel consist largely (~80%) of the same two unsaturated components. It is also worth noting that the cetane numbers of both biodiesel blends are close to 50, and the cetane numbers of methyl oleate and methyl linoleate are 59 and 38, respectively. Earlier, we observed that the differences in oxidation rates between RME and SME were greater in the atmospheric pressure JSR simulations (Fig. 9) than the differences in the 13.5 bar results shown in Fig. 10. Further study of the influences of operating conditions on ignition rates in these types of operating conditions could be very instructive. In particular, the results in both Fig. 9 and Fig. 10 describe stoichiometric fuel/oxidizer conditions, and relative ignition rates for rich mixtures might approach diesel ignition conditions better than stoichiometric mixtures.

Computed ignition delay times [41,55] for *n*-hexadecane are also shown as filled circles in Fig. 10; *n*-hexadecane is the reference fuel for cetane ratings, with a defined CN = 100.

These computed ignition delay values are significantly shorter than the values computed for methyl stearate or methyl palmitate. Finally, although not shown in the figure, computed ignition delay times for 2,2,4,4,6,8,8-heptamethyl nonane, the other primary reference fuel for cetane number with CN = 15, is slightly slower to ignite than methyl linoleate (CN=38) and slightly faster than methyl linolenate (CN = 23). At this time, with considerable uncertainties in the details of the present kinetic models for the methyl ester fuels, it is not possible to make strong statements concerning correlations between CN and computed ignition delay time. Individual shock tube ignition delay experiments for the 5 methyl ester fuel components of this study over the NTC region would be very valuable, in order to refine the mechanisms. In addition, it may be unreasonable to expect either JSR or shock tube ignition to have the same fuel-dependence as either cetane or octane numbers.

Reaction path analysis of the ignition of the 5 methyl esters provides additional guidance to those families of reactions that also need attention to refine the present modeling predictions. Each methyl ester begins to react following the arrival of the reflected shock wave, beginning with initiation via unimolecular decomposition and then reacting by H atom abstraction. The fuels with multiple C=C double bonds react preferentially via H atom abstraction at the allylic sites. For the early period of autoignition, and at the higher temperatures where the next reaction steps involve alkyl radical decomposition, uncertainties in the kinetic mechanism are relatively minor. At lower temperatures, molecular O_2 adds at the sites of the H atom abstraction, producing an alkyl ester version of RO_2 radicals, which then proceed to transfer H atoms internally via radical isomerization. This is the point where the

different numbers of C=C double bonds make a difference in the overall reaction rates of the methyl ester biodiesel fuel components.

Each RO_2 isomerization proceeds via a transition state ring that includes the C-O-O• as well as some number (i.e., 1, 2, 3, or 4) of C atoms in the long chain of the radical, and finally an H atom bonded to the target C atom. In alkane fuels, the rate of the isomerization depends on the number of C atoms in this transition state ring, and on the energy of the C-H bond that is broken by the internal abstraction by the RO_2. Different transition state rings have different contributions to ignition rates, because each ring size makes a different contribution to the overall rate of chain branching and chain propagation [68-72]. Transition state rings with 5 atoms, which abstract the H atom adjacent to the C-O-O• which is abstracting the H atom, lead almost entirely to chain propagation, producing mainly an olefin species and HO_2 radicals, and 6-membered transition state rings lead to products that decompose rapidly into one OH radical and two relatively stable intermediate species. Transition state rings with 7 atoms are most important for providing relatively stable QOOH radical intermediates, which can add to another O_2 molecule, then proceed to further isomerization reactions and ultimately to multiple small radical species, including 2 or more highly reactive OH radicals. These multiple radicals are thus responsible for most low temperature ignition of hydrocarbon and methyl ester hydrocarbon species.

When the transition state ring includes a C=C bond, the rate of the isomerization reaction is influenced, but there is relatively little guidance on the degree of this influence and how the double bond affects the internal abstraction at different types of sites (i.e., primary, secondary, tertiary, allylic, vinylic) from which the H atom is abstracted. In the recent work on

modeling kinetics of methyl decenoate with one double bond in the fuel molecule, Herbinet et al. [30] chose to add 15 kcal/mol to the activation energy of any isomerization reaction which contained a double bond, and that model did a very good job of predicting reliable kinetic behavior. In contrast, Mehl et al. [44], in a study of oxidation of the three structural isomers of hexene (C_6H_{12}), and Bounaceur et al. [46], in a study of the isomers of hexene and heptene, completely eliminated any such isomerization reactions that included a double bond, which is effectively giving that reaction a very large activation energy barrier due to the double bond.

In the present methyl ester mechanisms, the spacing of the double bonds is important, as seen in Fig. 1. In methyl linoleate, the two double bonds are separated by one C atom, at which the C-H bonds are "doubly" allylic, or very weakly bound. In methyl linolenate, the three double bonds are separated by two of the same type of "doubly allylic" C atom with low C-H bond energies. Abstraction of the first H atom from methyl linoleate or methyl linolenate is strongly preferential at these particular allylic sites, and molecular O_2 adds rapidly to these sites, which are notable because they are immediately adjacent to a C=C double bond on one side or both sides of the C-O-O* that has been produced. If the double bond had no effect on the isomerization reactions, then the H atom on the other side of the double bond would participate in an isomerization reaction with a 7-membered transition state ring and an H atom with a very weak allylic bond to its C atom, making the isomerization extremely rapid. When we tested this assumption by artifically making the double bond have zero effect on the energy barrier for isomerization, these 7-membered transition state rings dominated the ignition kinetics, resulting in predictions of ignition for methyl linolenate that were as much as 100 times faster than those values in Figure 10. We continued to increase the activation energy

barrier due to the C=C double bond being embedded in the 7-membered transition state ring, always finding ignition to be extremely fast. Only by completely eliminating these isomerization reactions that contained the double bond were we able to predict ignition for methyl linolenate that was slower than that for the other methyl esters being studied. Therefore, the present mechanisms have such reactions excluded entirely, in agreement with recent studies [44,46].

Clearly, there are two major reaction classes where much more information is needed, and which could be addressed through theoretical tools now available. The first class is the isomerization across a C=C double bond to refine model predictions for such reactions. Most significant would be the estimation of the energy barrier due to the embedded double bond. The second type of reaction for which model refinement is needed and which should be accessible at present is the nature and rate of the addition of O_2 to an allylic site in molecules like these methyl esters. If the dissociation reaction to R + O_2 is faster than our thermochemical treatments are predicting, then the isomerization of these RO_2 species would be less important, since the enhanced dissociation of the RO_2 adduct to R + O_2 would reduce the isomerization rates by lowering the concentrations of the adducts. The present assumption that such reactions are very slow results in predicted ignition delay times that are consistent with the limited observations available for mechanism validation, but this reaction sequence needs considerable further attention.

FUTURE MECHANISM DEVELOPMENTS

In addition to the contribution of these C=C double bonds to the present mechanisms, there are many kinetic elements of the present mechanism where refinements would be

helpful and plans are being made for improvements. A collaboration with Dean and Carstensen [73] is in place to refine all of the R + O_2 and subsequent alkylperoxy radical isomerization reaction pathways and reaction rates. Since the current mechanisms reproduce the features and extent of the NTC region for hydrocarbon and other species including the present large methyl ester fuels, we are confident that, even with its known limitations, the present and related kinetic mechanisms accurately predict the correct relative contributions of chain branching and chain propagation rates in the NTC regime, and the refinements being planned must be able to reproduce that balance following the upgrading of the mechanisms. We are continuing to refine the modeling details of the second generation intermediate species, particularly the olefin species produced by alkane oxidation. Past mechanisms have lumped the olefin kinetics in a way that cannot accurately predict olefin consumption or species-specific product distributions that are becoming more important than in the past. We also continue to work on refinements in the small-molecule core mechanism that is common to all hydrocarbon and related fuel oxidation.

Mechanisms like the present methyl ester model continue to evolve as more detail becomes available from theory and experiments, or when new species begin to be important as major components of a fuel mixture, such as in a surrogate mechanism for a practical fuel [74-76]. It is instructive to note that the first kinetic models of methyl ester fuels, with a goal of understanding biodiesel fuel combustion, appeared about 10 years ago, and nearly all of the kinetic models of methyl ester fuels larger than methyl butanoate have been developed in the past 5 years. This is a very active, dynamic subject area, strongly enabled by rapid growth in

computing power. This rapid progress is a demonstration of how quickly progress can be made in a challenging subject area when so many researchers collectively focus their attention on it.

ACKNOWLEDGMENTS

The authors thank Mr. Nathan Barnes for his assistance in carrying out some of the calculations used in this paper. This work was supported in part by the US Department of Energy, Office of Vehicle Technologies, and the authors thank program managers Gurpreet Singh and Kevin Stork for their support. This work was performed under the auspices of the US Department of Energy by Lawrence Livermore National Laboratory under Contract DE-AC52-07NA27344.

REFERENCES

1. M.S. Graboski, R.L. McCormick, Prog. Energy Combust. Sci. 24 (1998) 125-164.

2. K. Bozbas, Renew. Sust. Energy Rev. 12 (2) (2008) 542-552.

3. N. Miyamoto, H. Ogawa, N.M. Nurun, K. Obata, T. Arima, SAE Technical Paper Series, 980506 (1998).

4. C.K. Westbrook, W.J. Pitz, H.J. Curran, J. Phys. Chem. A 110 (2006) 6912-6922.

5. A.K. Agarwal, Prog. Energy Combust. Sci. 33 (2007) 233-271.

6. M. Lapuerta, O. Armas, J. Rodriguez-Fernandez, Prog. Energy Combust. Sci. 34 (2008) 198-223.

7. J.G. Wallis, J.L. Watts, J. Browse, Trends Biochem. Sci. 27 (9) (2002) 467-473.

8. C.S. Alexander, M. Ratcliff, National Renewable Energy Laboratory report NREL/MP-540-43696 (2008).

9. A. Schönborn, N. Ladommatos, J. Williams, R. Allan, J. Rogerson, Combust. Flame 156 (2009) 1396-1412.

10. J.P. Szybist, A.L. Boehman, D.C. Haworth, H. Koga, Combust. Flame 149 (1-2) (2007) 112-128.

11. J.P. Szybist, J. Song, M. Alam, A.L. Boehman, Fuel Process. Technol. 88 (7) (2007) 679-691.

12. Y. Zhang, Y. Yang, A.L. Boehman, Combust. Flame 156 (2009) 1202-1213.

13. B.I. Parsons, C.J. Danby, J. Chem. Soc. (1956) 1795-1798.

14. E.M. Fisher, W.J. Pitz, H.J. Curran, C.K. Westbrook, Proc. Combust. Inst. 28 (2000) 1579-1586.

15. W.K. Metcalfe, S. Dooley, H.J. Curran, J.M. Simmie, A.M. El-Nahas, M.V. Navarro, J. Phys. Chem. 111 (19) (2007) 4001-4014.

16. S. Gaïl, M.J. Thomson, S.M. Sarathy, S.A. Syed, P. Dagaut, P. Dievart, A.J. Marchese, F.L. Dryer, Proc. Combust. Inst. 31 (1) (2007) 305-3011.

17. T. Vaughan, M. Hammill, M. Harris, A.J. Marchese, SAE Technical Paper Series, 2006-01-3302.

18. S. Gaïl, S.M. Sarathy, M.J. Thomson, P. Dievart, P. Dagaut, Combust. Flame 155 (2008) 635-650.

19. A. Farooq, D.F. Davidson, R.K. Hanson, L.K. Huynh, A. Violi, Proc. Combust. Inst. 32 (2009) 247-253.

20. S.M. Walton, M.S. Wooldridge, C.K. Westbrook, Proc. Combust. Inst. 32 (2009) 255-262.

21. S. Dooley, H.J. Curran, J.M. Simmie, Combust. Flame 153 (2008) 2-32.

22. C.K. Westbrook, W.J. Pitz, P.R. Westmoreland, F.L. Dryer, M. Chaos, P. Osswald, K. Kohse-Höinghaus, T.A. Cool, J. Wang, B. Yang, N. Hansen, T. Kasper, Proc. Combust. Inst. 32 (2009) 221-228.

23. L. Gasnot, V. Decottignies, J.F. Pauwels, Fuel 84 (2005) 505-518.

24. K. Hadj-Ali, M. Crochet, G. Vanhove, M. Ribaucour, R. Minetti, Proc. Combust. Inst. 32 (2009) 239-246.

25. G. Dayma, S. Gail, P. Dagaut, Energy Fuel 22 (3) (2008) 1469-1479.

26. G. Dayma, C. Togbe, P. Dagaut, Energy Fuel 23 (9) (2009 4254-4268.

27. J. Biet, V. Warth, O. Herbinet, P.A. Glaude, F. Battin-Leclerc, Proc. Fourth Europ. Combust. Meeting (2009).

28. P.A. Glaude, O. Herbinet, S. Bax, J. Biet, V. Warth, F. Battin-Leclerc, Combust. Flame (2010), doi: 10.1016/j.combustflame.2010.03.012.

29. O. Herbinet, W.J. Pitz, C.K. Westbrook, Combust. Flame 154 (2008) 507-528.

30. O. Herbinet, W.J. Pitz, C.K. Westbrook, Combust. Flame 157 (2010) 893-908.

31. S.M. Sarathy, M.J. Thomson, W.J. Pitz, T. Lu, Proc. Combust. Inst. 33, in press (2011).

32. K. Seshadri, T. Lu, O. Herbinet, S. Humer, U. Niemann, W.J. Pitz, R. Seiser, C.K. Law, Proc. Combust. Inst. 32 (2009) 1067-1074.

33. H.P. Ramirez, L.K. Hadj-Ali, P. Dievart, G. Dayma, C. Togbe, G. Moreac, P. Dagaut, Proc. Combust. Inst. 33, in press (2011).

34. P. Dagaut, S. Gail, M. Sahasrabudhe, Proc. Combust. Inst. 31 (2007) 2955-2961.

35. P. Dagaut, S. Gail, J. Phys. Chem. A 111 (2007) 3992-4000.

36. O. Herbinet, J. Biet, M.H. Hakka, V. Warth, P.A. Glaude, A. Nicolle, F. Battin-Leclerc, Proc. Combust. Inst. 33, in press (2011).

37. C.M. Naik, C.K. Westbrook, O. Herbinet, W.J. Pitz, M. Mehl, Proc. Combust. Inst. (2010), doi:10.1016/j.proci.2010.05.007.

38. Y.Zhang, A.L. Boehman, Combust. Flame 157 (2010) 546-555.

39. H.J. Curran, P. Gaffuri, W.J. Pitz, C.K. Westbrook, Combust. Flame 114 (1998) 149-177.

40. H.J. Curran, P. Gaffuri, W.J. Pitz, C.K. Westbrook, Combust. Flame 129 (2002) 253-280.

41. C.K. Westbrook, W.J. Pitz, O. Herbinet, H.J. Curran, E.J. Silke, Combust. Flame 156 (2009) 181-199.

42. D.F. Davidson, J.T. Herbon, D.C. Horning, R.K. Horning, Int. J. Chem. Kinet. 33 (2001) 775-783.

43. U. Pfahl, K. Fieweger, G. Adomeit, Proc. Combust. Inst. 26 (1996) 781-789.

44. M. Mehl, G. Vanhove, W.J. Pitz, E. Ranzi, Combust. Flame 155 (2008) 756-772.

45. G. Vanhove, M. Ribaucour, R. Minetti, Proc. Combust. Inst. 30 (2005) 1065-1072.

46. R. Bounaceur, V. Warth, B. Sirjean, P.A. Glaude, R. Fournet, F. Battin-Leclerc, Proc. Combust. Inst. 32 (2009) 387-394.

47. M.H. Hakka, P.A. Glaude, O. Herbinet, F. Battin-Leclerc, Combust. Flame 156 (2009) 2129-2144.

48. S. Bax, M.H. Hakka, P.A. Glaude, O. Herbinet, F. Battin-Leclerc, Combust. Flame 157 (2010) 1220-1229.

49. G. Knothe, Prog. Energy Combust. Sci. 36 (2010) 364-373.

50. J.Y.W. Lai, K.C. Lin, A. Violi, Prog. Energy Combust. Sci. (2010), doi:10.1016/j.pecs.2010.03.001.

51. G. Bourque, D. Healy, H.J. Curran, C. Zinner, D. Kalitan, J. de Vries, C. Aul, E. Petersen, Proc. ASME Turbo Expo. 3 (2008) 1051-1066.

52. M. O'Conaire, H.J. Curran, J.M. Simmie, W.J. Pitz, C.K. Westbrook, Int. J. Chem. Kinet. 36 (2004) 603-622.

53. J. Li, Z. Zhao, A. Kazakov, F.L. Dryer, Int. J. Chem. Kinet. 36 (2004) 566-575.

54. M.A. Oehlschlaeger, J. Steinberg, C.K. Westbrook, W.J. Pitz, Combust. Flame 156 (2009) 2165-2172.

55. C.K. Westbrook, W.J. Pitz, M. Mehl, H.J. Curran, Proc. Combust. Inst. 33 (2010), doi:10.1016/j.proci.2010.05-087.

56. F. Battin-Leclerc, R. Bounaceur, G.M. Come, R. Fournet, P.-A. Glaude, G. Scacchi, V. Warth, EXGAS-ALKANES: A Software for the Automatic Generation of Mechanisms for the Oxidation of Alkanes, CNRS (2004).

57. F. Battin-Leclerc, Prog. Energy Combust. Sci. 34 (2008) 440-498.

58. J. Biet, M.H. Hakka, V. Warth, P.-A. Glaude, F. Battin-Leclerc, Energy Fuel 22 (2008) 2258-2269.

59. A. Osmont, M. Yahyaoui, L. Catoire, I. Gokalp, M.T. Swihart, Combust. Flame 155 (2008) 334-342.

60. H.J. Curran, Int. J. Chem. Kinet. 38 (2006) 250-275.

61. R.T. Pollard, Comprehensive Chemical Kinetics, Vol. 17, (C.H. Bamford and C.F.H. Tipper, Eds.), Elsevier, New York, 1977.

62. Chemkin MFC-3.5, Reaction Design: San Diego, California (2009).

63. J. Van Gerpen, B. Shanks, R. Pruszko, D. Clements, G. Knothe, Biodiesel Production Technology, National Renewable Energy Laboratory Report NREL/SR-510-36244, 2004.

64. Y. Stein, R.A. Yetter, F.L. Dryer, A. Aradi, SAE Technical Paper Series, 1999-01-1504.

65. National Biofuels Group, url=http://www.natbiogroup.com/default.asp?id=66

66. H.K. Ciezki, G. Adomeit, Combust. Flame 93 (1993) 421-433.

67. K. Fieweger, R. Blumenthal, G. Adomeit, Combust. Flame 109 (1997) 599-619.

68. J. Zador, C.A. Taatjes, R.X. Fernandes, Prog. Energy Combust. Sci. (2010) doi:10.1016/j.pecs/2010.06.006.

69. F. Battin-Leclerc, O. Herbinet, P.-A. Glaude, R. Fournet, Z. Zhou, L. Deng, Angew. Chem. Int. Ed. 49 (2010) 3169-3172.

70. J.F. Griffiths, S.K. Scott, Prog. Energy Combust. Sci. 13 (1987) 161-197.

71. J.F. Griffiths, Combust. Flame 93 (1993) 202-206.

72. C.K. Westbrook, W.J. Pitz, W.R. Leppard, SAE Technical Paper Series, 912314 (1991).

73. H.-H. Carstensen, A.M. Dean, Comprehensive Chemical Kinetics 42 (2007) 105-187.

74. W.J. Pitz, N.P. Cernansky, F.L. Dryer, F.N. Egolfopoulos, J.T. Farrell, D.G. Friend, H. Pitsch, SAE Technical Paper Series, 2007-01-0175 (2007).

75. J.T. Farrell, N.P. Cernansky, F.L. Dryer, D.G. Friend, C.A. Hergart, C.K. Law, R.M. McDavid, C.J. Mueller, A.K. Patel, H. Pitsch, SAE Technical Paper Series, 2007-01-0201 (2007).

76. M. Colket, T. Edwards, S. Williams, N.P. Cernansky, D.L. Miller, F. Egolfopoulos, P. Lindstedt, K. Seshadri, F.L. Dryer, C.K. Law, D. Friend, D.B. Lenhert, H. Pitsch, A. Sarofim, M. Smooke, W. Tsang, AIAA publication AIAA-2007-0770, 2007.

Table caption

1. Compositions for rapeseed methyl ester (RME) fuel and soy methyl ester (SME) fuel, as fractions of the five individual methyl esters in this study. Also shown are the measured cetane numbers (CN) for each of the fuel components and the Derived Cetane Number determined [ref] by the Ignition Quality Tester.

Figure captions

1. Diagrams of the structure of 4 biodiesel fuel components, showing the nature of the carbon/carbon bonds (single vs. double bonds). The naming system used in the modeling is shown, both the site index number at the bottom of each carbon chain, and the type of carbon/hydrogen atom bond at each location.

2. Fractional conversion of methyl palmitate and *n*-decane in a JSR. Lines are computed results for methyl palmitate (solid line) and *n*-decane (dashed line), symbols show measured values from Hakka et al. [47] for methyl palmitate (diamonds) and *n*-decane (triangles). Mixture has 0.002 total mole fraction fuel (0.26 methyl palmitate/0.74 *n*-decane), stoichiometric with O_2, diluted by helium, atmospheric pressure.

3. Comparisons between experimental results from Hakka et al. [47] (symbols) and computed values (lines) for selected 1-olefin species with the conditions shown in Fig. 2.

4. Comparisons between experimental results from Hakka et al. [47] (symbols) and computed values (lines) for selected 1-olefin methyl ester species with the conditions shown in Fig. 2.

5. Fractional conversion of methyl oleate and n-decane in a JSR. Lines are computed results for methyl oleate (solid line) and *n*-decane (dashed line), symbols show measured values from Bax et al. [48] for methyl oleate (diamonds) and *n*-decane (triangles). Mixture has 0.002 total mole fraction fuel (0.26 methyl oleate/0.74 *n*-decane), stoichiometric with O_2, diluted by helium, atmospheric pressure.

6. Comparisons between experimental results from Bax et al. [48] (symbols) and computed values (lines) for selected major intermediate species with the conditions shown in Fig. 5.

7. Comparisons between experimental results (symbols) from Dagaut et al. [34] and computed results for RME oxidation in JSR at 10 bar pressure, stoichiometric RME/O_2 with 0.05% fuel, diluted in N_2 and with a residence time of 1 second. Also shown are computed fractional fuel conversions for methyl oleate (solid curve) and methyl palmitate (dashed curve).

8. Computed fuel fractional conversions for 5 separate simulations, each with a different methyl ester fuel. The fuel in each case is given in the legend, for stoichiometric fuel/oxygen, 0.5% fuel, with helium diluent, residence time 1.5s.

9. Computed comparison between oxidation of RME and SME in a simulated JSR, stoichiometric fuel/oxygen, 0.5% fuel, diluted in helium, residence time 1.5s. The RME and SME compositions taken from Table 1.

10. Ignition delay times for stoichiometric fuel/air mixtures in a reflected shock environment, 13.5 bar initial pressure. Experimental results [66] for n-heptane/air are shown by asterisks, other results are kinetic model predictions. Lines show predicted values for each methyl ester fuel, circles for n-cetane [41], squares and diamonds are predictions for SME and RME.

Table

Table 1

Ester		Fraction of RME	Fraction of SME	Cetane Number (CN)	Derived Cetane Number (DCN)
Methyl palmitate	$C_{17}H_{34}O_2$	4.3	6-10	86	
Methyl stearate	$C_{19}H_{38}O_2$	1.3	2-5	101	95.6
Methyl oleate	$C_{19}H_{36}O_2$	59.9	20-30	59	59.3
Methyl linoleate	$C_{19}H_{34}O_2$	21.1	50-60	38	42.6
Methyl linolenate	$C_{19}H_{32}O_2$	13.2	5-11	23	36.1

Figure

(a) methyl stearate

p s s s s s s s s s s s s s s s_{co} **O** p

C - C - C - C - C - C - C - C - C - C - C - C - C - C - C - C - C - O - C

18 17 16 15 14 13 12 11 10 9 8 7 6 5 4 3 2 m

(b) methyl oleate

p s s s s s s a v v a s s s s s s_{co} **O** p

C - C - C - C - C - C - C - C - C = C - C - C - C - C - C - C - C - C - O - C

18 17 16 15 14 13 12 11 10 9 8 7 6 5 4 3 2 m

(c) methyl linoleate

p s s s a v v a v v a s s s s s s_{co} **O** p

C - C - C - C - C - C = C - C - C = C - C - C - C - C - C - C - C - C - O - C

18 17 16 15 14 13 12 11 10 9 8 7 6 5 4 3 2 m

(d) methyl linolenate

p a v v a v v a v v a s s s s s s_{co} **O** p

C - C - C = C - C - C = C - C - C = C - C - C - C - C - C - C - C - C - O - C

18 17 16 15 14 13 12 11 10 9 8 7 6 5 4 3 2 m

Figure 1

Figure

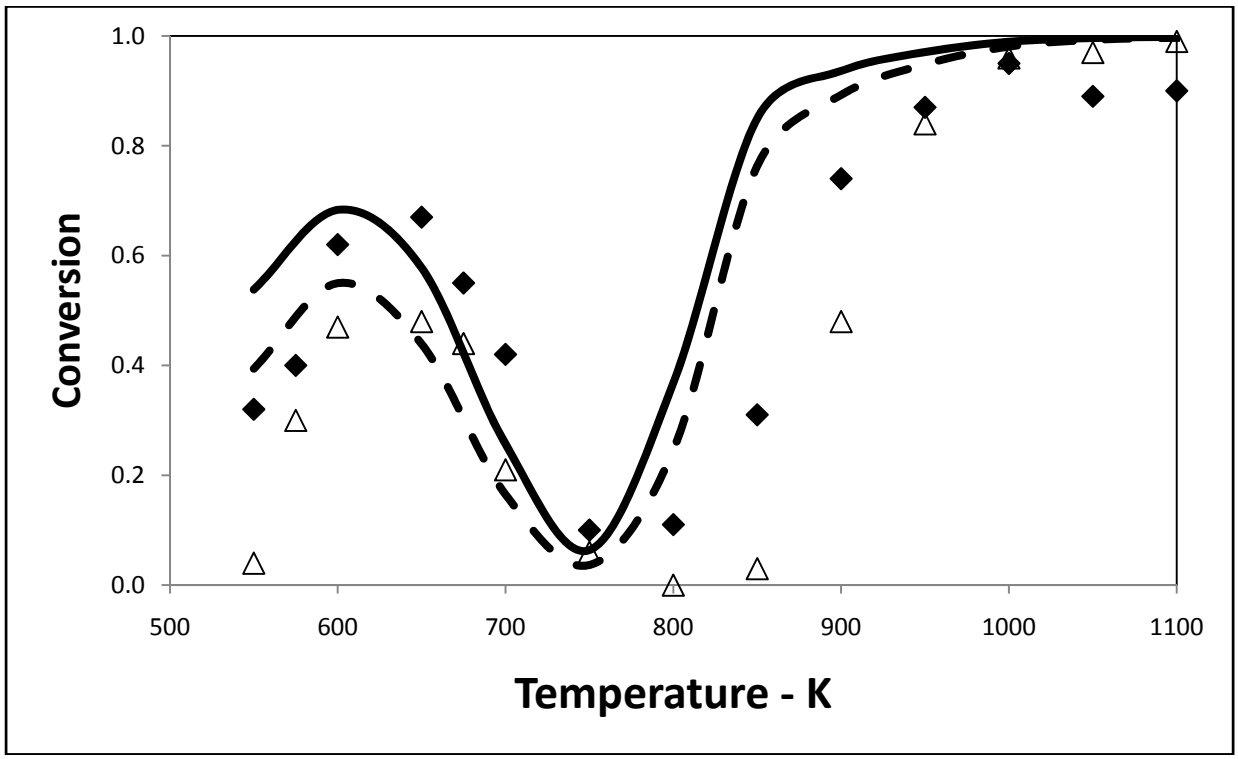

Figure 2

Figure

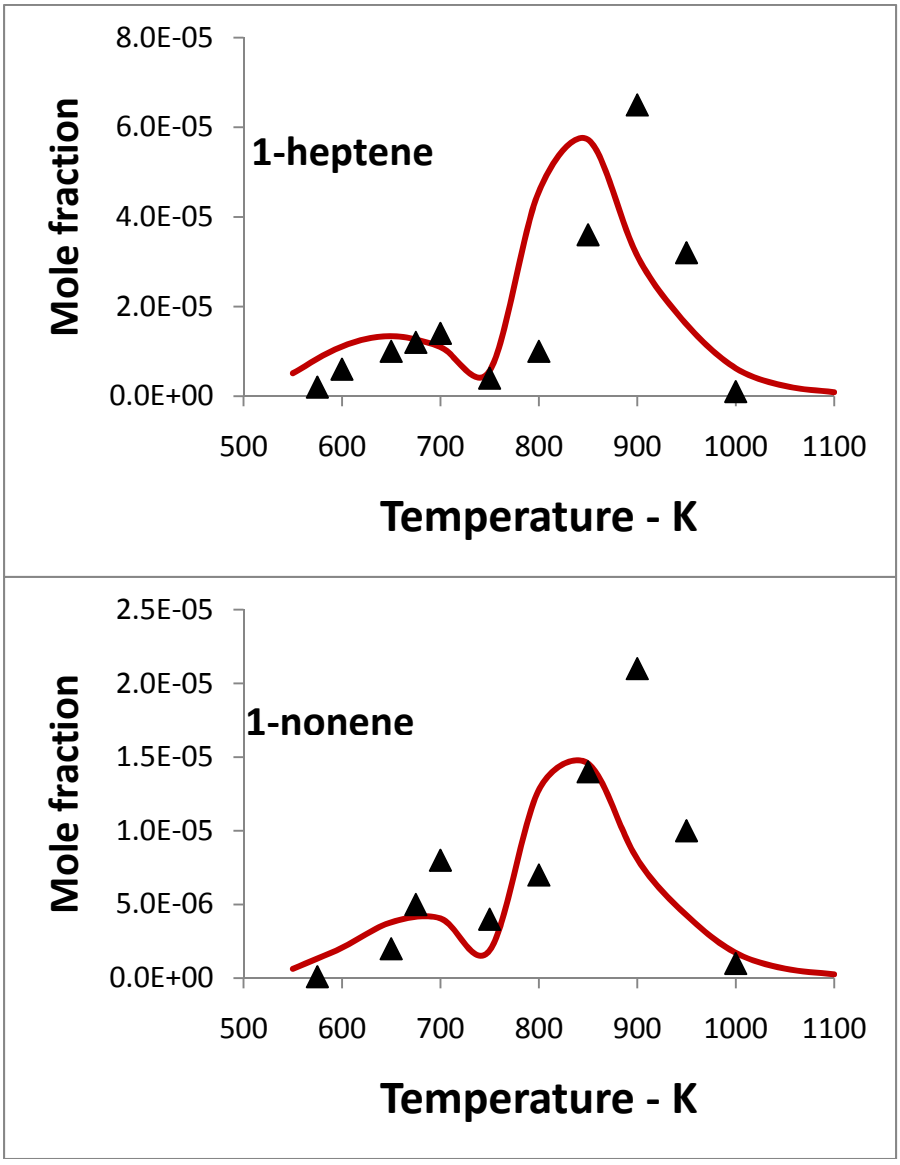

Figure 3a

Figure

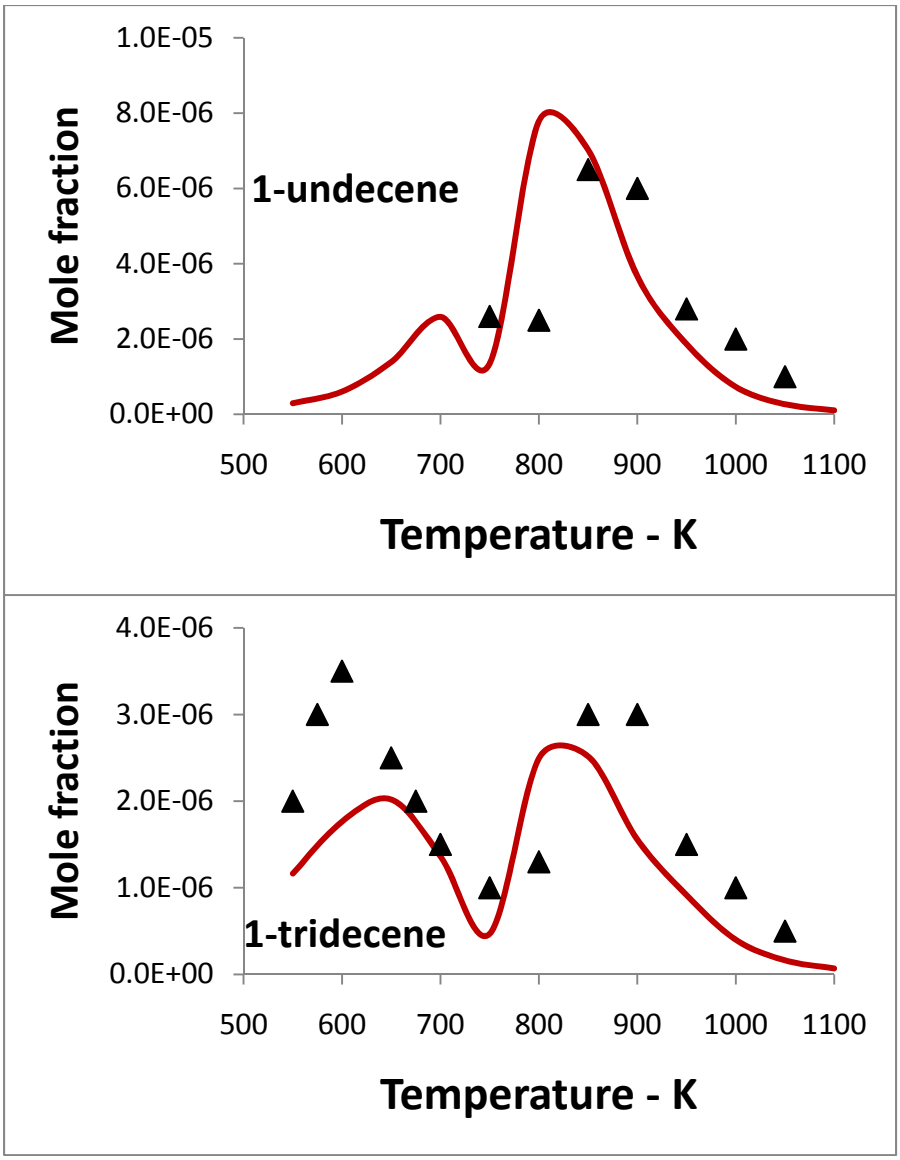

Figure 3b

Figure

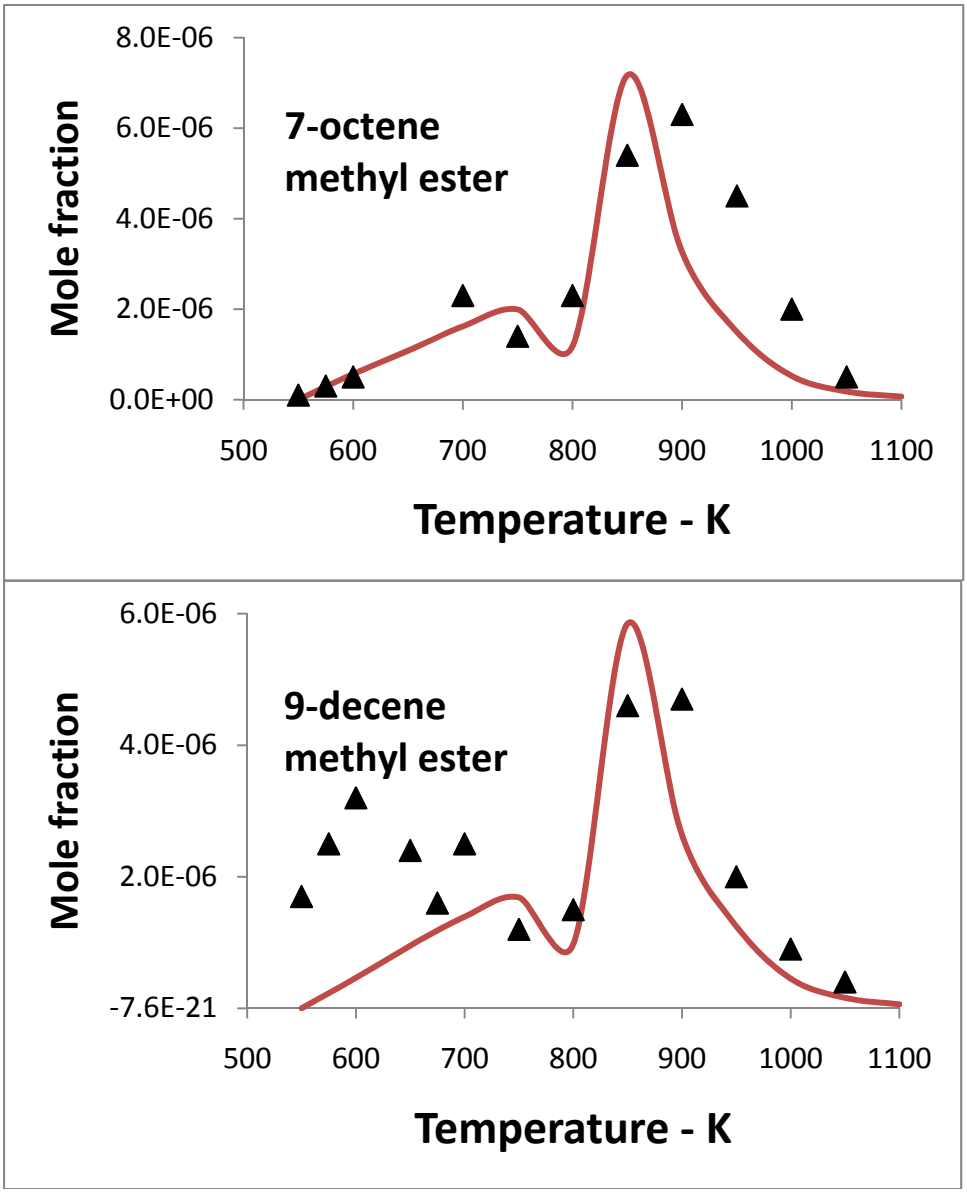

Figure 4a

Figure

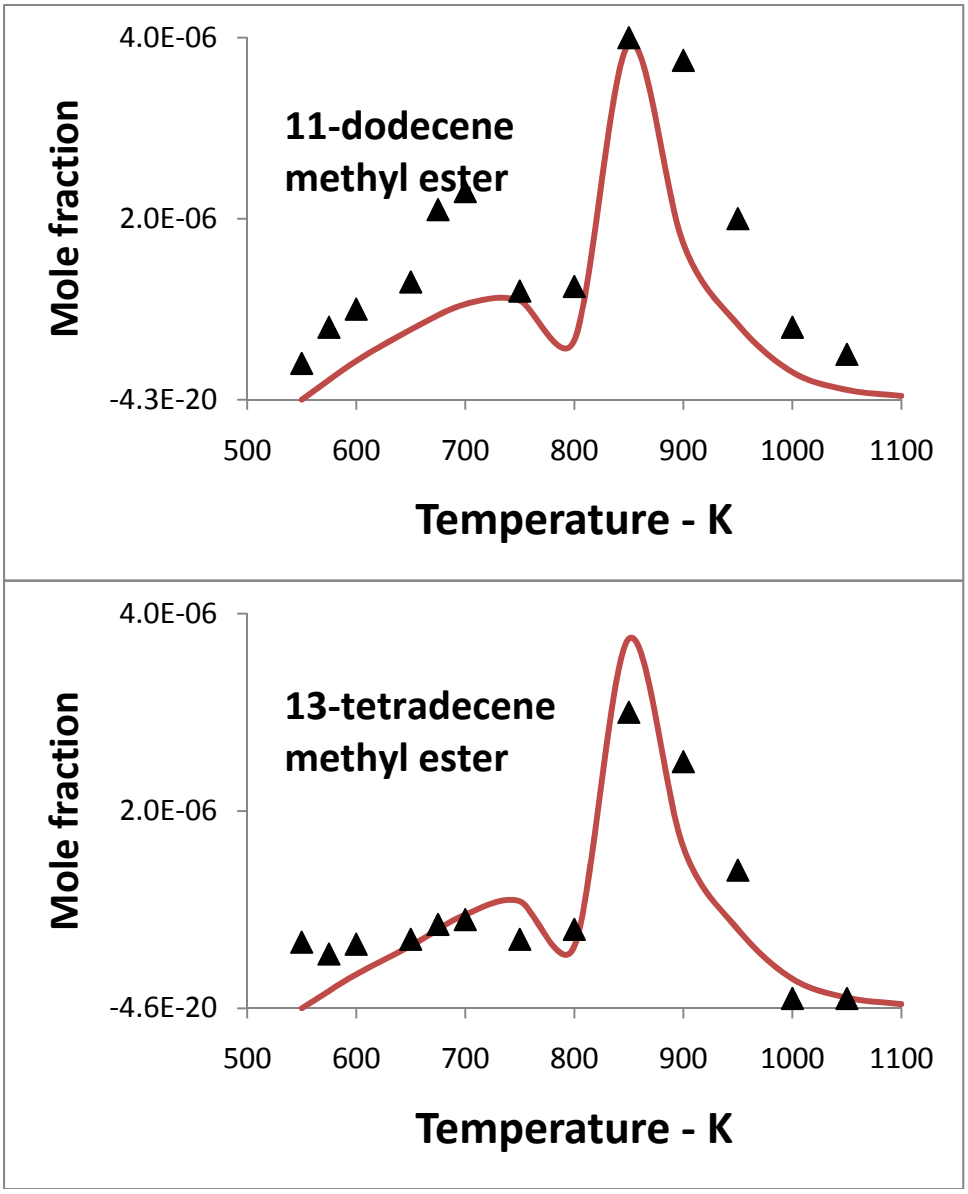

Figure 4b

Figure

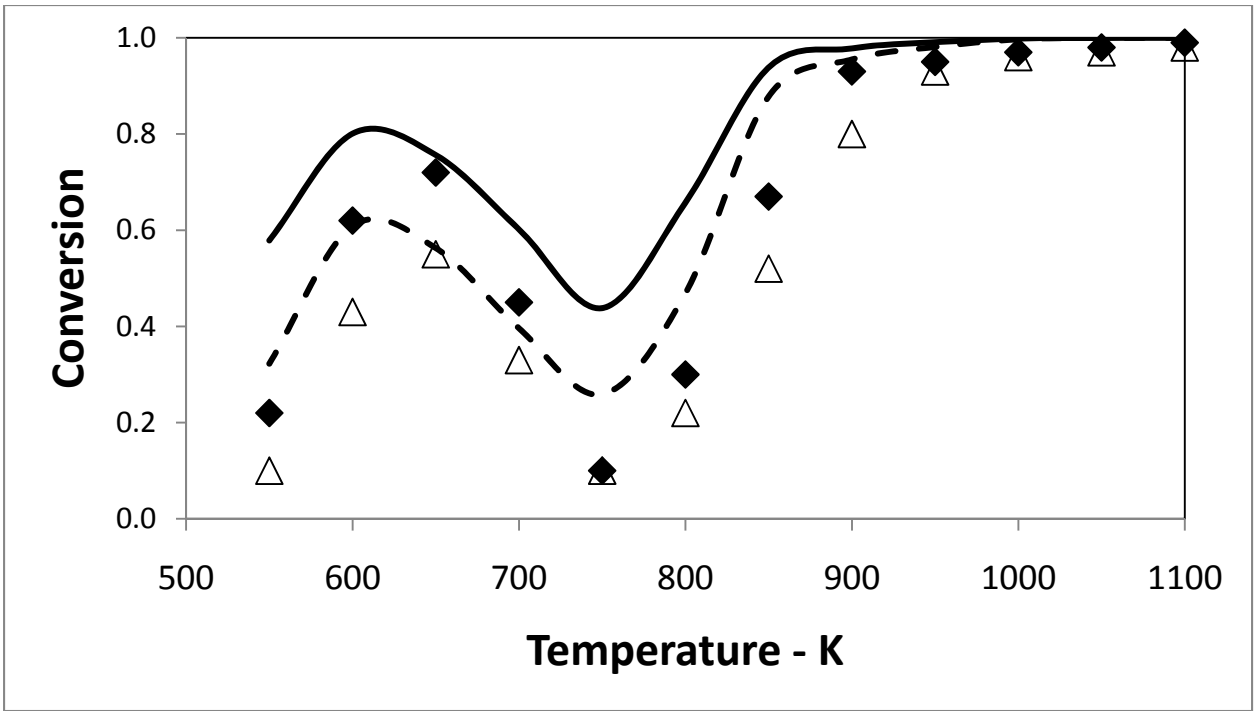

Figure 5

Figure

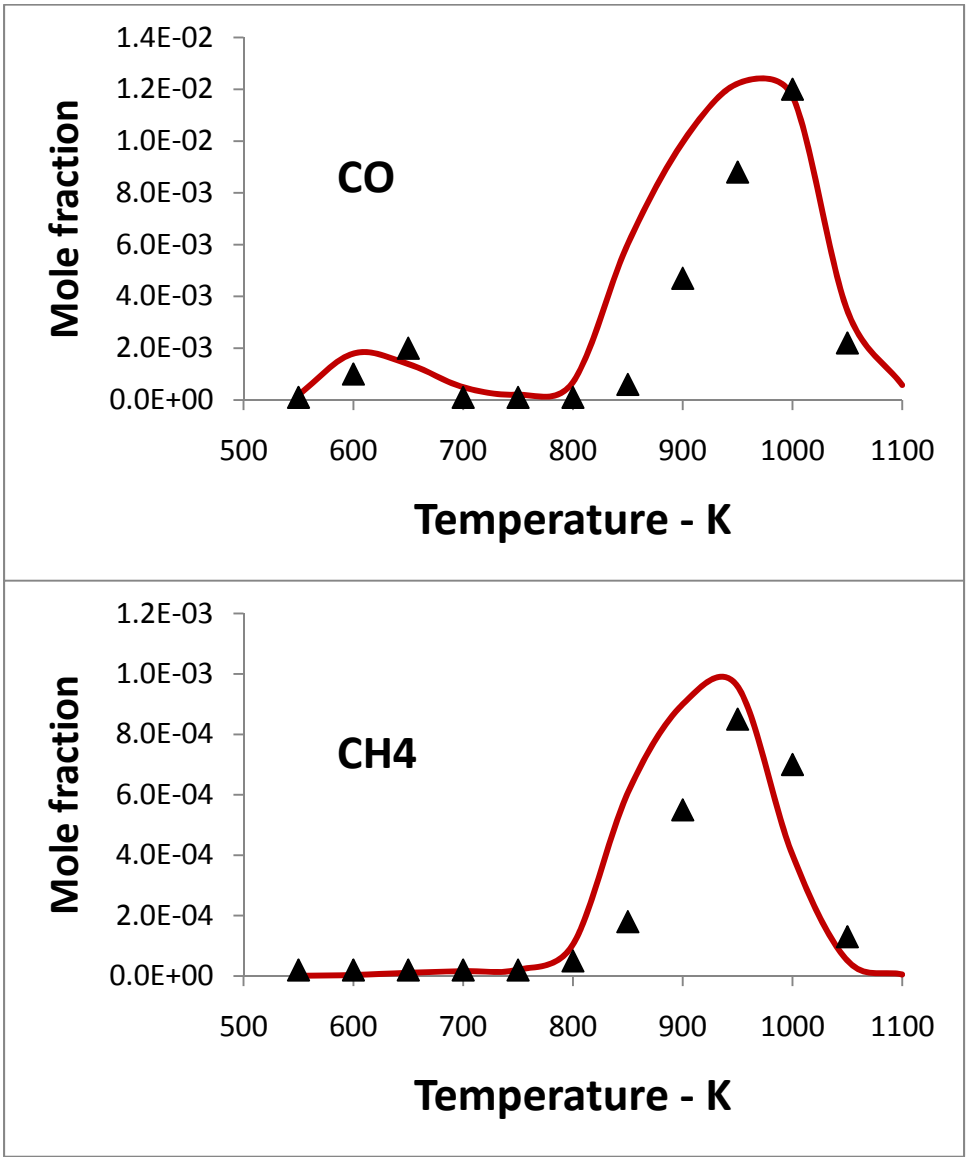

Figure 6a

Figure

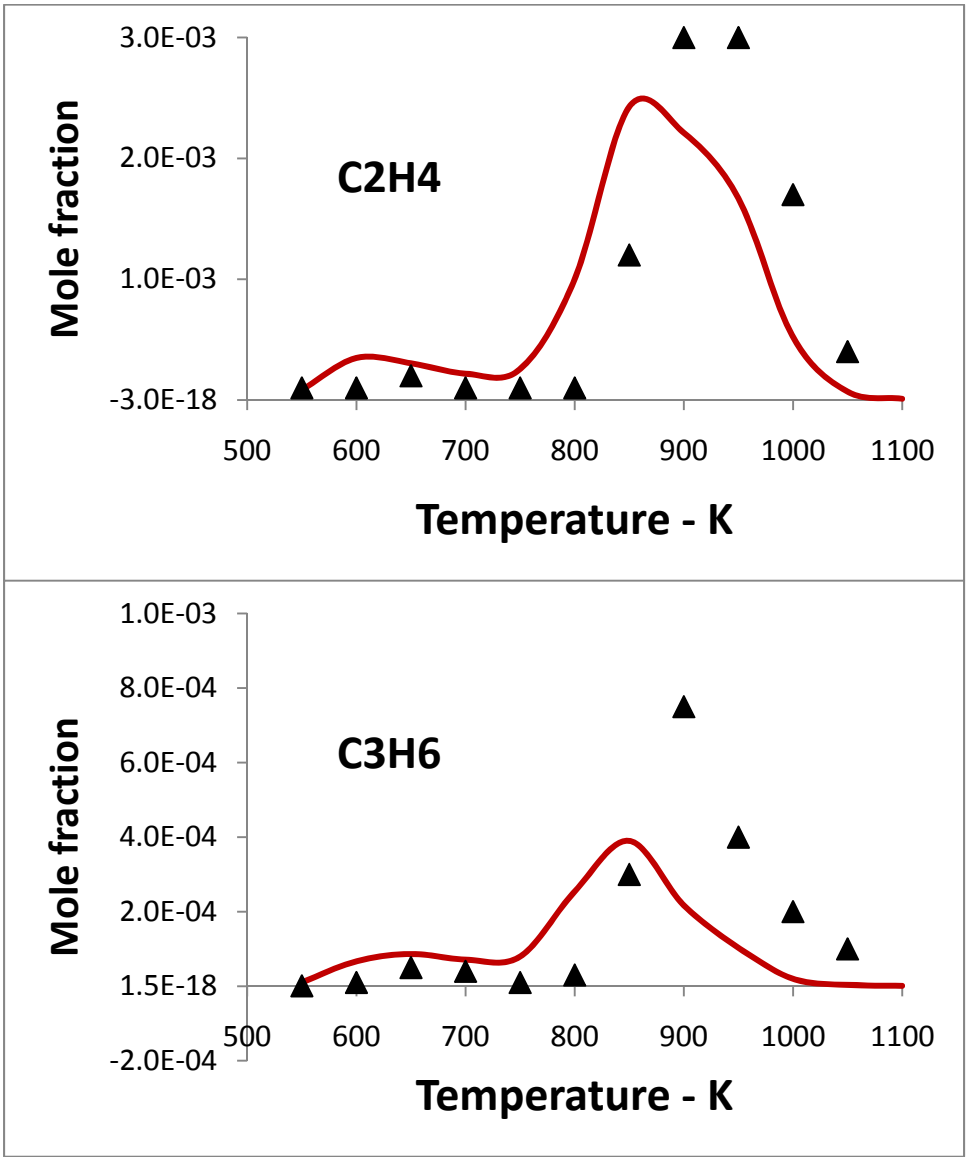

Figure 6b

Figure

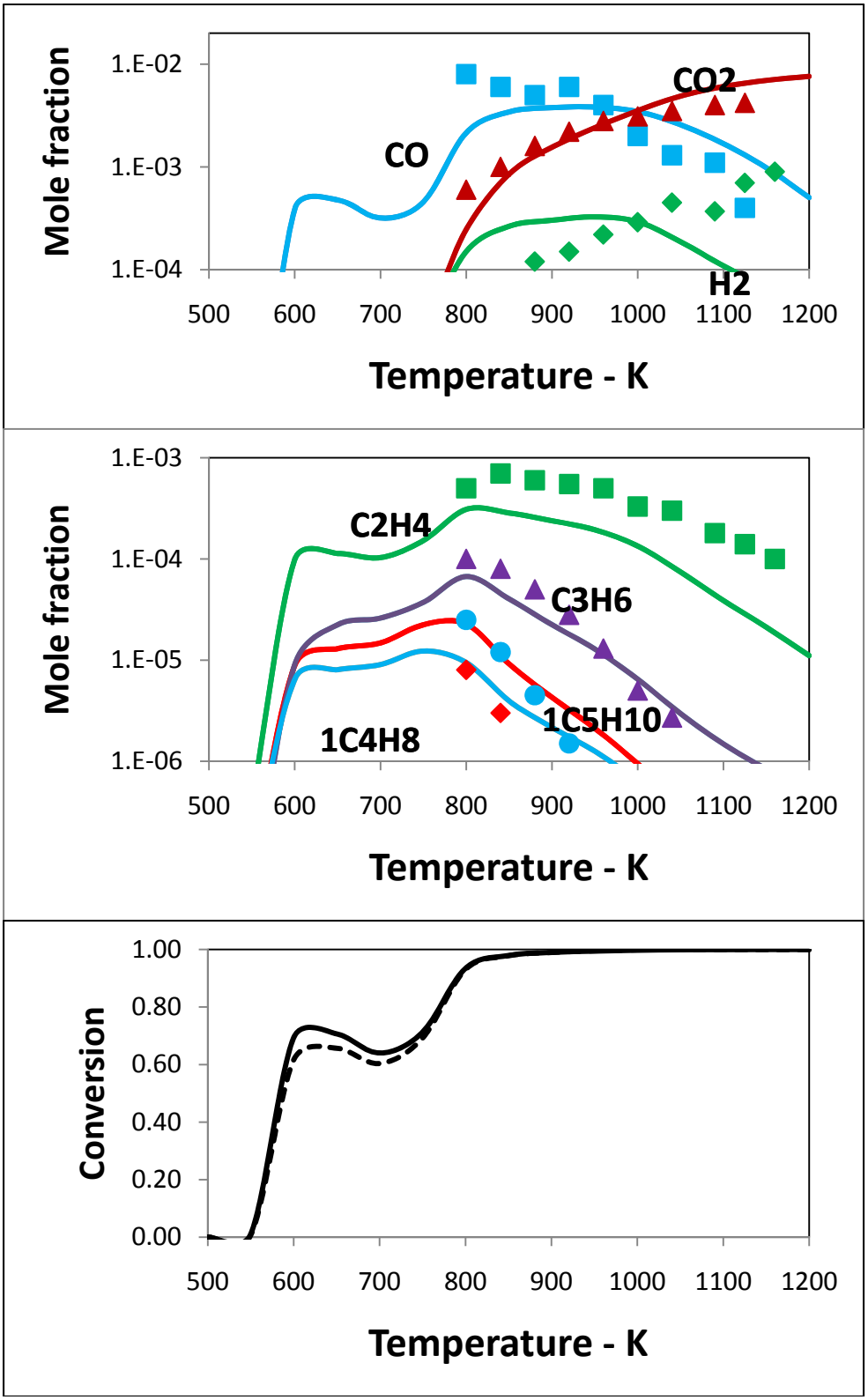

Figure 7

Figure

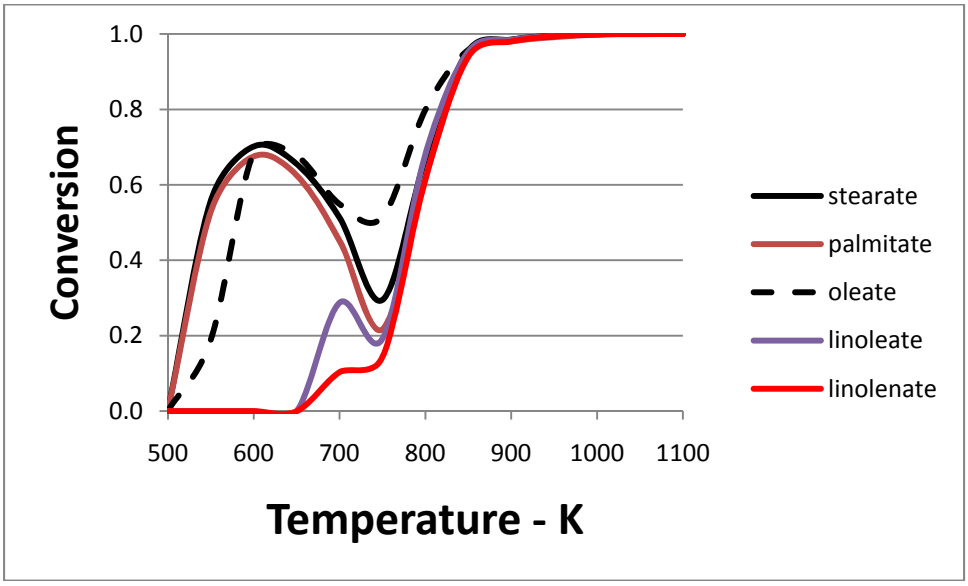

Figure 8

Figure

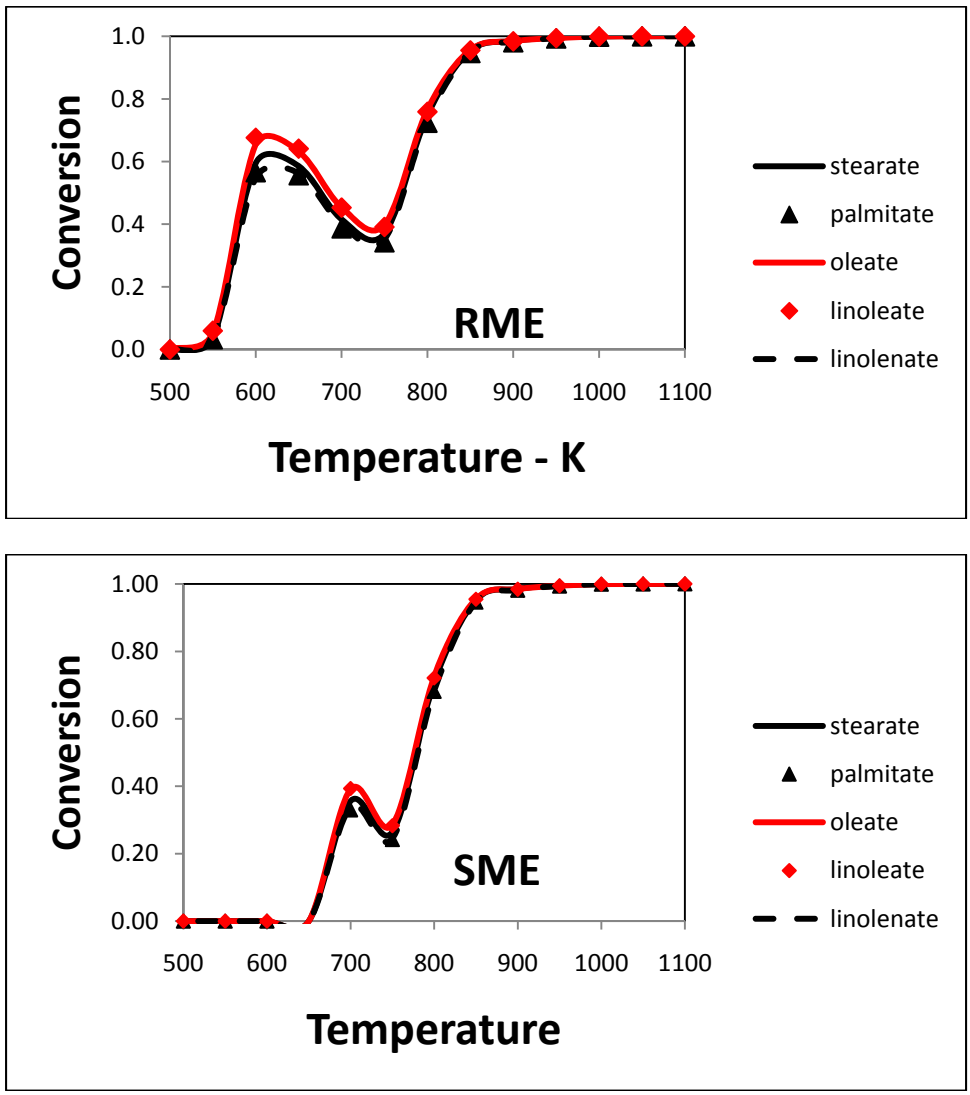

Figure 9

Figure

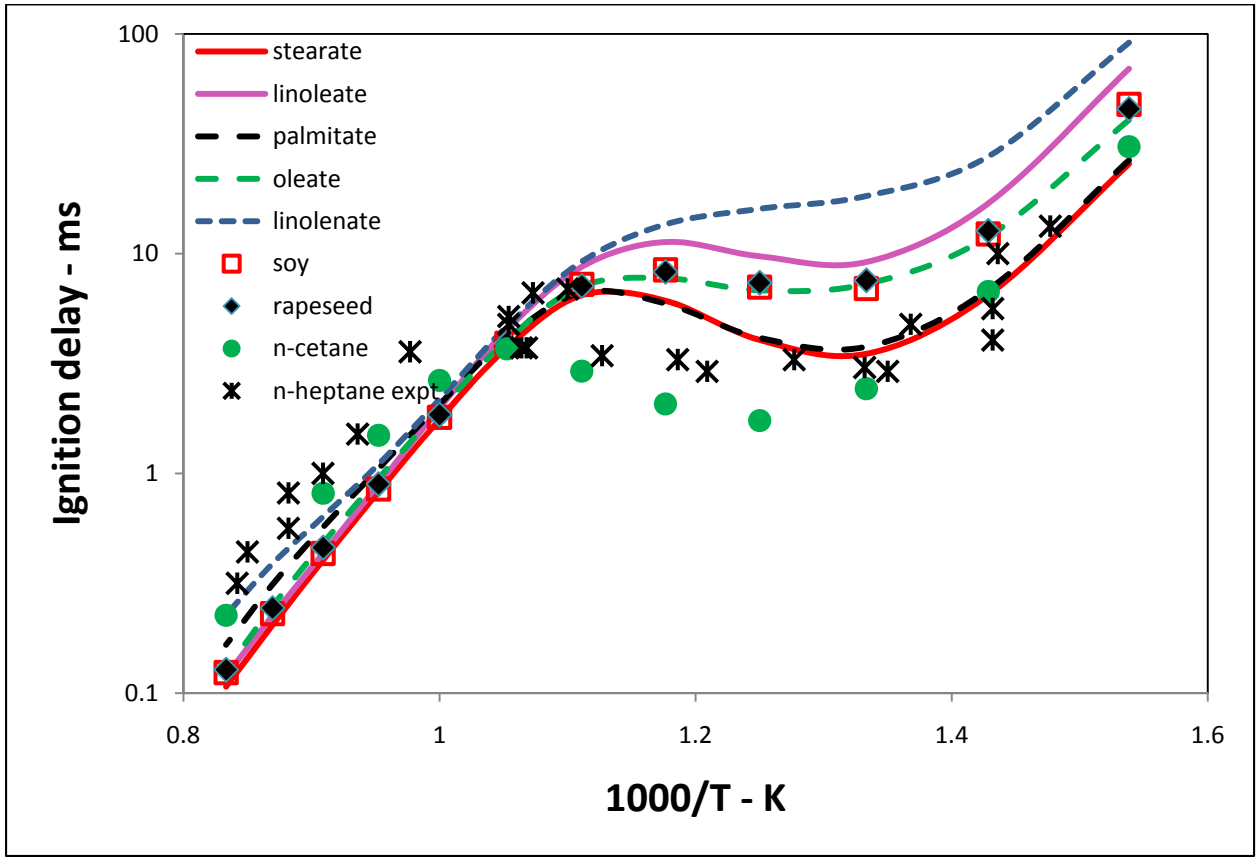

Figure 10